ABSTRACT

A 2D Electrical Resistivity Survey of Palsas in Tavvavuoma, sub-arctic Sweden.

Per Marklund

Electrical resistivity tomography (ERT) is a commonly used geophysical method to investigate permafrost in the mountain environment, but few studies have employed this method in a permafrost affected peatland. For this thesis, 5 ERT profiles were measured over 17 palsas and peat-plateaus in a palsa peatland environment in Tavvavuoma, northern Sweden, where the primary aim was to investigate the depth to the base of permafrost under the mounds. These depths are also used to estimate the excess ice fraction (EIF), which is indicative of the proportion of segregation ice in the frozen core under the mounds. The internal structure of palsas and the spatial distribution of permafrost was also investigated from the inverted resistivity models.

Permafrost thickness was found to range from 5 – 17 m, with the thickest permafrost in the west end of the study area. EIF values range between 0,04 to 0,58, with the lowest values in the same end as the deepest permafrost, where also low mound elevations are found. The deep permafrost combined with low mound elevations are suggested to be attributed to the presence of coarse grained (glaciofluvial) sediments where ice segregation formation is limited, thus small amounts of frost heave. Deep permafrost is possibly underlying at least two thermokarst depressions/fens in the area, which is suggested to obstruct their drainage. The height of the mounds was surprisingly found to decrease with permafrost thickness, a relationship that is likely to be an effect of the varied underlying sediment cover. This thesis demonstrates the applicability of ERT in peatland permafrost research, but also considers the limitations of the method.

Keywords: Palsas, peat plateaus, resistivity, ert, geophysics, Tavvavuoma

SAMMANFATTNING

Undersökning av palsar med hjälp av elektrisk resistivitetstomografi i Tavvavuoma, norra Sverige.

Per Marklund

Elektrisk resistivitetstomografi (ERT) är en geofysisk metod som har använts flitigt vid undersökningar av alpin permafrost, men få studier har hittills tillämpat denna teknik vid undersökningar av permafrost i myrmarker. Under detta examensarbete på masternivå mättes 5 ERT-profiler över 17 palsar samt torvplatåer i ett palsmyrkomplex med sporadisk permafrost i Tavvavuoma, norra Sverige, med det primära målet att undersöka permafrostens mäktighet under dessa. De beräknade permafrostdjupen används även för att uppskatta isöverskottsfraktionen (EIF), vilket ger en indikation på andelen segregationsis i den frusna kärnan under respektive pals/torvplatå. Palsarnas interna struktur och den rumsliga utbredningen av permafrost i myren diskuteras också kvalitativt utifrån resistivitetsmodellerna.

Permafrostmäktigheten under palsar och torvplatåer bestämdes till mellan 5 – 17 meter, med den djupaste permafrosten i den västra delen av studieområdet. Isöverskottsfraktionen varierar mellan 0,04 – 0,58, med de lägsta värdena i samma del av studieområdet som den djupaste permafrosten fanns, här är även palshöjderna låga. Den djupa permafrosten i kombination med låga palshöjder föreslås tillskrivas förekomst av grovkorniga (glaciofluviala) sediment i denna del av studieområdet, där bildningen av segregationsis begränsas. I och med detta begränsas mängden frosthävning, med låga palshöjder som resultat. Djup permafrost kan finnas under minst två thermokarstsänkor i området, vilket kan hindra dränering av dessa. Ett oväntat resultat var att palshöjd minskar med ökat permafrostdjup bland de studerade objekten, vilket bäst kan förklaras med det varierade sedimentunderlaget, som ger mycket olika förutsättningar för segregationsisbildning. Denna masteruppsats visar på tillämpligheten av ERT i myrmarker med permafrost, men beaktar även metodens begränsningar för denna tillämpning.

Nyckelord: Palsar, torvplatåer, resistivitet, ert, geofysik, Tavvavuoma

Table of Contents

1 INTRODUCTION

1.1 BACKGROUND

The term 'palsa' originates from the Finnish and Saami languages and is describing a "hummock rising out of a bog with a core of ice" (Seppälä, 1972). This type of landform is a typical feature of the discontinuous permafrost zone of the northern hemisphere, and often defines the margin of continental permafrost occurrence (Seppälä, 1986; Sollid and Sørbel, 1998). Since northern Sweden lies on the fringe of permafrost occurrence in the northern hemisphere (Brown et al., 1997), it is of particular interest to study permafrost distribution, the environmental and climatic factors controlling it, and the occurrence of permafrost related landforms in this region, where frozen ground often is found to be close to the point of thawing (E.g. Christiansen et al., 2010).

The thermal properties of peat allow permafrost to persist in the peatlands of the marginal permafrost zones. Dry peat has about the same thermal properties as snow, i.e. insulating (E.g. French, 2007). This means that during the dry part of summer, ground ice is protected from the summer heat, and is prevented from excessive thaw. When peat is wet however, it can conduct heat better, which means that during winter when temperature is low and the isolating snow cover on top of the elevated palsas is thin, the peat bog which has been saturated with moisture during the storms of the past autumn can now effectively conduct heat away from the palsa surface and build the frozen core.

Palsas undergo a cyclic evolution, with a development and decay that are strongly controlled by climatic parameters (Seppälä, 1986), and thus changes in the distribution of palsas can indicate changes in permafrost boundaries related to climate change (Sollid and Sørbel, 1998; Zuidhoff and Kolstrup, 2000). Individual collapsing palsas are however not a sign of climate change, it is a continuous phenomenon and an inherent part of the cyclic evolution of palsas. A general decay of palsas can however indicate a change in climate (Zuidhoff 2003).

Earlier morphology studies on palsas (E.g. Seppälä, 1986; Wramner, 1973; Åhman, 1977) have in many cases been limited due to the inaccessible interior of palsas and the high work effort and/or costs needed to drill. In this study, the non-destructive and comparably inexpensive geophysical method of electrical resistivity tomography (ERT) is used on palsas and peat plateaus where recent measurements suggest that palsas are close to thawing (Christiansen et al., 2010). This is done to learn about the thickness of permafrost, the ice content of

the frozen core and to image the details of the palsas internal structure. This information can then be used to understand both past and current processes in the palsa mire, factors controlling permafrost occurrence and thickness, and the state of permafrost in this marginal permafrost zone.

1.2 OBJECTIVES

In this master thesis the spatial distribution and characteristics of permafrost in palsas and peat plateaus of Tavvavuoma are studied with the use of 2-dimensional electrical resistivity tomography (ERT), with the primary aims to:

1. Determine the thickness of permafrost in the surveyed mounds. Depth is determined by inverse modeling of the 2D resistivity measurements.
2. Estimate the excess ice content using the excess ice fraction (EIF), which is calculated from the depth to the permafrost base acquired from the resistivity models. EIF is a measure of the proportion of surplus ice present in the palsa, which is greater than the amount of moisture the soil would be able to hold under non-frozen conditions.
3. Analyze the internal structure of the palsas, and the extent of permafrost, from the inverse 2D resistivity models.

The results from the survey will be used to discuss the possible processes in the palsa bog, the controls of permafrost thickness and distribution, and also to briefly discuss the use and reliability of ERT in these types of environments.

1.3 Site Description

Tavvavuoma (*Northern Saami: Dávvavuopmi*) (*68°28′N, 20°54′E*) is a large peatland-complex within the sporadic permafrost zone, situated in a flat basin approximately 200 km^2 wide at approximately 550 m.a.s.l. in northern-most sub-arctic Sweden (Figure 1).

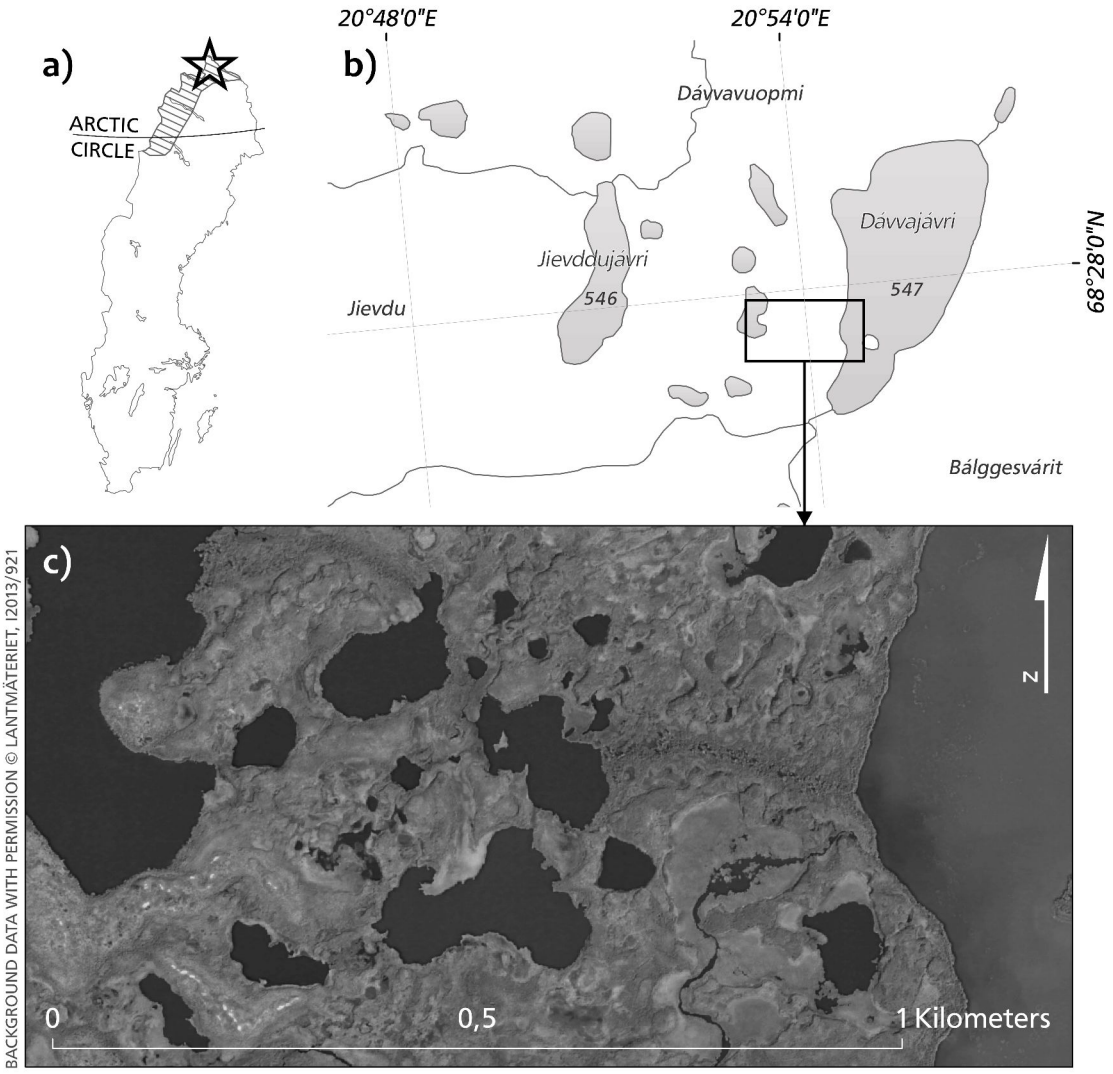

Figure 1: Tavvavuoma. a) Geographic location of study area (indicated by star). Zone of palsa distribution in Sweden is indicated by dashed area, drawn from Rapp and Annersten (1969). b) Overview of Tavvavuoma. c) Close-up of study site.

This is one of the most extensive areas of palsas, peat plateaus and thermokarst lakes found within the sporadic permafrost zone of northern Fennoscandia (Sannel and Kuhry, 2010). The area has also been proposed as a new national park by the Swedish Environmental Protection Agency, due in part to its

uniquely rich bird life, in addition to the high concentration of palsas found here (Naturvårdsverket, 2008).

The site where the study is conducted (Figure 1c) is located just west of Tavvajaure (*Northern Saami: Dávvajávri*) and covers less than 0,5 km^2 with palsas and peat plateaus, ranging from approximately 0,5 – 4 meters above the mire surface.

1.3.1 Geology

Bedrock is mainly found in outcrop on the mountain sides surrounding the study area. It consists of the Svekofennian basement (1,7 – 2,8 Ga), with mainly felsic intrusives (e.g. granites), often gneissic (Geological Survey of Sweden, internet). Bedrock of the younger Caledonian orogeny (The Scandinavian mountain range) is not a part of the study area as it ends west of Tavvavuoma.

The quaternary glacial deposits are mostly covered with peat at the surveyed area, except on the western end where some ridge-formed glaciofluvial material is exposed on the surface (Lagerbäck, 2012). Hempel (2009) suggest that a fen developed at the site at approximately 10,100 years B.P., and that the transition to bog peat mire with permafrost formation probably occurred at around 250 – 100 B.P., i.e. during the little ice-age. The average depth to mineral sediments from the peat surface is about 1,6 meters (Sannel and Kuhry, 2011).

1.3.2 Vegetation

The vegetation in the fens is dominated by sedges (*Carex* spp.), cottongrass (*Eriophorum angustifolium*) (Figure 2b, 2c), and peat mosses (*Sphagnum* spp.). On the much drier top of palsas and peat plateaus the vegetation is replaced by species that can handle the lesser amount of available soil moisture, such as mulberries (*Rubus chamaemorus*) (Figure 2d), crowberries (*Empetrum hermaphroditum*), dwarf birch (*Betula nana*), and juniper haircap moss (*Polytrichum junipernium*). The flat top of wind exposed palsas are commonly stripped of the vegetation layer by wind erosion, with bare peat exposed (Figure 2a) (Wramner, 1973).

Mountain birch (*Betula pubescens* ssp. *czerepanovii*) is found on the gently sloping hills surrounding the peatland, as well as on some locations within the mires where mineral soil is exposed and along watercourses. Downy willows (*Salix lapponum*) also line the flanks of the watercourses.

Figure 2: Vegetation in the palsa mire. a) Palsa with wind eroded top surface. b) Vegetation infill of thaw pond. c) Cottongrass (*Eriophorum angustifolium*) on lake shore. d) Mullberries (*Rubus chamaemorus*) on the dry top of palsa.

1.3.3 Climate

The closest weather station to Tavvavuoma is Naimakka (Approx. 40 km to north-east), but the temperature series for the station in Karesuando (Approx. 65 km to the east) stretches further back in time, starting in 1879 A.D., and has previously been used for determining the climate for Tavvavuoma (Sannel and Kuhry, 2011). Here the mean annual air temperature (MAAT) for the standard period 1961 – 1990 is -2,3°C. For the later 1971 – 2000 period, a warmer -1,9°C was noted. For Naimakka the MAAT (1961 – 1990) is -2,6°C (Swedish Meteorological and Hydrological Institute, Internet).

Tavvavuoma is in average 1,2°C colder than recorded temperatures at Karesuando (at 327 m.a.s.l), based on recent records starting in 2005 in Tavvavuoma (Sannel and Kuhry, 2011). This temperature difference is mainly due to the difference in altitude between the sites. The valley floor may also be subjected to strong temperature inversions, indicated by a 'double tree-line' on the adjacent mountain slopes (Wramner, 1973), where the lowest part of the hillslopes lacks or has an irregular occurrence of mountain birch vegetation,

while it is denser in up-slope direction.

Mean annual precipitation in Karesuando for the 1961 – 1990 period is 416 mm, and for the winter months (November – April), when most of the precipitation fall as snow, is 143 mm (Swedish Meteorological and Hydrological Institute, Internet). For the later 1971 – 2000 period a mean annual precipitation of 451 mm is reported, and for the winter months 152 mm (Swedish Meteorological and Hydrological Institute, Internet).

1.4 Previous studies in Tavvavuoma

Geomorphological studies of palsas have been conducted through a number of doctoral theses, reports and articles from different sites in northern Sweden, Norway and Finland (E.g. Åhman, 1977; Zuidhoff 2003; Seppälä 1986; Wramner 1973; Sollid and Sørbel, 1998). The earliest detailed studies of palsas in the Tavvavuoma basin was conducted by Per Wramner during the 1960s and 1970s (Wramner, 1965; 1968; 1972; 1973). Wramners sites are all situated between 3 – 11 kilometers north-west of the current study site. Wramners investigations were focused on morphology, morphological processes and genesis of palsas with the use of coring, sediment analyses and morphological observations/mappings over a decade. Cyclic evolution of palsas was one of the conclusions, and that the most important erosion process is by 'block erosion'. During this time Wramner also observed embryonic stage- and growing palsas in the mire.

Climatic parameters (Air temperature, precipitation, humidity, wind direction and wind speed), thermokarst erosion rates and ground temperatures have been monitored at the site since September 2005 (Britta Sannel, personal communication). The ground temperature data from the boreholes show that permafrost temperatures are close to thawing at -0,3°C (Christiansen et al., 2010). A comparative study was made by Sannel and Kuhry (2011) between Tavvavuoma, the Hudson Bay lowlands (Canada) and Rogovaya (Russia), focusing on the peatplateau/thermokarst lake dynamics. By analyzing aerial photography and high resolution satellite images they could show that the formation of new thermokarst lakes was highest in Tavvavuoma of the three sites.

Geophysical surveys with ground penetrating radar (GPR) have previously been conducted in Tavvavuoma by Maria Tuomi (unpublished), which showed that ground ice lenses and permafrost boundaries are clearly detectable by GPR. Ylva Sjöberg is currently mapping permafrost table depths in the palsa bog with the use of GPR, to validate results from hydrological permafrost modeling (Ylva Sjöberg, personal communication).

1.5 Palsa morphology & Genesis

Palsas are small peat-mounds with a permanently frozen core, which are most commonly found in the discontinuous permafrost zone (Seppälä, 2011; Åhman, 1977; Lundqvist, 1969). The frozen core can consist of peat and/or sediments, but common for all palsas is the overlying cover of peat. Layers of segregated ice within the frozen core raise the palsa above the surrounding topography. Palsas typically vary in height between 1 to 7 meters, and are less than 100 meters in diameter (French, 2007).

The formation of ice segregation layers in the palsa core is caused by water moving towards the freezing plane when water expands as it freezes. The water migrates because the free energy of the unfrozen water is lowered when the pressure increases due to the ice expansion, hence the water will move towards the low pressure freezing plane of the ice layer (Hohmann, 1997). This effect is sometimes called 'cryosuction'. The phenomenon requires that the soil has small enough interstices to keep the pressure gradient maintained, thus finer grained sediments are more prone to form ice segregation layers, and these sediments are termed 'frost-susceptible'. If the substrate is not frost-susceptible the water will freeze *in situ* as pore ice (French, 2007).

The definition of palsas has been wildly discussed in the literature (Gurney, 2001). The controversy is mainly regarding whether peat is required for the term palsa to apply. So called 'mineral palsas' and 'organic palsas' (Pissart and Gangloff, 1984) was introduced to explain frost mounds in mineral soils and organic soils respectively. Other authors state that palsas are a landform occurring exclusively in peat bogs, thus a cover of peat is an essential component (E.g. Seppälä, 1972). The term 'lithalsa' has later replaced 'mineral palsa' (Pissart, 2002) to reduce the confusion (French, 2007). Figure 3 shows the possible variations of palsa-like mounds with a frozen core.

Palsas are climate-induced morphological features, formed by freezing from above, with a cyclic evolution (Seppälä, 1986). The climatic conditions that characterize occurrence of palsas are not fully understood, due to sparse long-term meteorological data from remote palsa mire locations, and from the regions where they occur in whole (Seppälä, 2011). In general, the climatic conditions required are a MAAT below, and usually lower, than 0°C, and in addition low winter temperatures are needed. A thin snow cover during winter is needed to allow for frost penetration, but enough precipitation during summer to recharge the peat-mire with moisture (Seppälä, 2011).

Important to the development is the cyclic evolution that palsas undergo, collapse of single palsas are not necessarily a sign of climate change, but is an inherent property of their evolution. A general degradation within an area can

however indicate a change in climate (E.g. Zuidhoff, 2003).

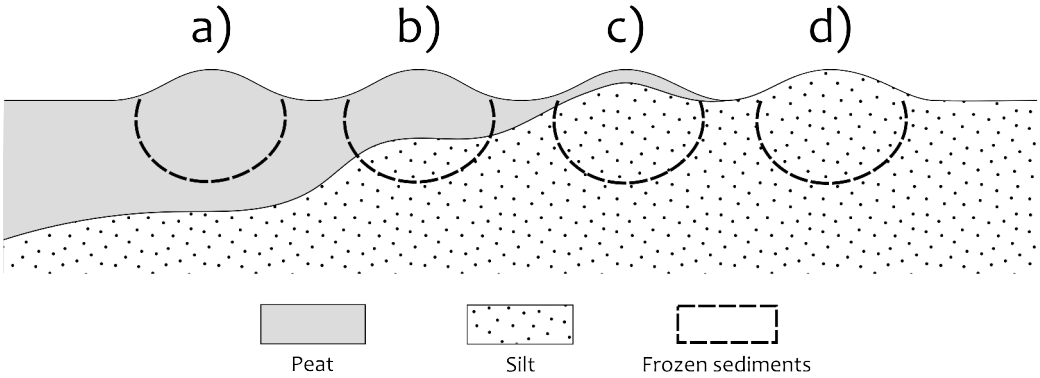

Figure 3: Different types of palsa like frost mounds. a) Palsa formed entierly in peat. b) Peat palsa, with ice core extending down into sediments. c) Mineral-cored palsa with a cover of peat, most ice-segregation is within the sediments. d) Mineral permafrost mound, "lithalsa". Redrawn from Gurney (2001).

The initiation of palsa development, the first steps in the creation of the 'palsa embryo', is the most problematic part of the genesis of palsas. As explained by Seppälä (1986; 2011), palsa formation starts with a local thinning of the snow cover due to wind drift. The loss of isolation from the snow cover means that heat more rapidly leaves the saturated peat surface, which has a high thermal conductivity. The surface of the mire rises as the freezing water expands, producing the palsa embryo (Figure 4b). Vegetation now changes on the palsa surface due desiccation. This means that less drifting snow is trapped by vegetation on top of the palsa. The dry peat on the surface of the palsa protects the ice core from the summer heat, as dry peat has low thermal conductivity. The autumn rains recharge the peat with moisture so that the winter cold can penetrate the peat layer and further develop the frozen core. After several winters the palsa has reached mature stage (Figure 4d) and can be up to 10 meters in height (French, 2007).

The collapse of a palsa can start when cracks form on the surface and edges and peat blocks break loose and fall into the pool of water that surround the palsa (Figure 4e). A slow melting from the bottom is another type of collapse, where the palsa is slowly lowered into the water, a small cupola is seen in the late stage standing out from the pool as it sinks. The circular pool created when the palsa is completely thawed (Figure 4f), is progressively filled with new peat, and new palsas may now emerge and the cycle may start over.

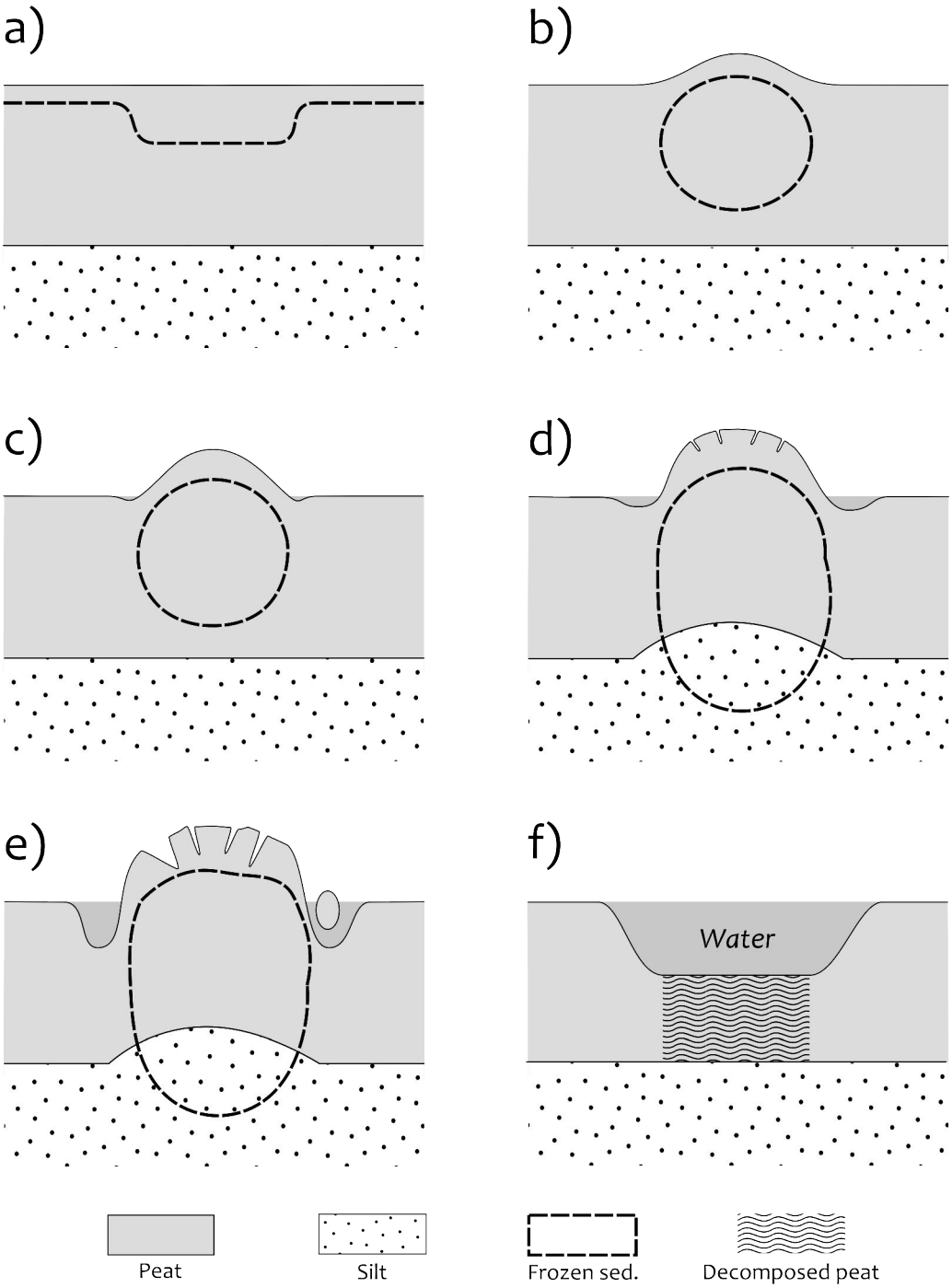

Figure 4: The cyclic development of a palsa. a) First winter. b) The palsa embryo, first summer. c) Young palsa. d) Mature palsa. e) Old and collapsing palsa. f) Fully thawed palsa. Extensively redrawn from Seppälä (1986).

1.5.1 Ice segregation & Excess ice

Layers of segregated ice in the underlying, often fine-grained, mineral sediments are thought to be an important component of palsa morphology, as

they raise the palsa above the surrounding topography (French, 2007). Laboratory studies have shown that ice segregation within peat is unlikely however (Kujala et al., 2008), therefore ice lenses found in drillings of peat (E.g. Åhman, 1977; Seppälä, 1988) might not be possible to explain by ice segregation. Ice segregation in the mineral sediments has also been indicated to be the most important process for growth of palsas in Tavvavuoma (Wramner, 1973: p.80).

The formation of segregated ice layers creates an excess of ice, increasing the total volume of the frozen ground. The amount of water is now exceeding that amount of water the ground would be able to hold under non-frozen conditions. An implication of this is that thawing of ground with excess ice will lead to ground subsidence, as the excess ice melts and the water drains. This is a big concern when constructing on frozen ground, since ground subsidence during thaw can cause significant damages on buildings and pipe-lines etc., if not planned for properly.

Excess ice content is often described as a percentage of the total volume, or 'excess ice fraction' (EIF). The advantage of expressing excess ice as a fraction of the total volume is that it indicates the potential morphological changes that would occur during thaw of the feature (French, 2007).

Lewkowicz et al. (2011) presented a formula, shown below, to calculate the EIF based on the height of a permafrost mound and the depth to the permafrost base.

$$EIF = \frac{h}{(d-a)} \tag{1}$$

Where h is the palsa elevation above the surrounding surface elevation, d is the depth to the permafrost base, and a is the thickness of the active layer.

1.6 Frozen ground geophysics

The use of geophysics in permafrost and frozen ground research is common today, and many advances have been made in developing the methods since the early days (Kneisel et al., 2008). Many physical material properties, such as resistivity, seismic velocity and dielectric permittivity etc., changes when water change from liquid to solid phase, and it is due to these changes in properties between the frozen/non-frozen ground that makes the distribution of permafrost possible to detect by geophysical methods.

The advantages of using geophysics are many. It can be used to map the subsurface conditions continuously over large areas, and it can depict the

subsurface conditions to a depth of a few tens of meters in most cases. Usually this can be made to a much lower cost compared to borehole drillings. Though the value of direct observations in the form of expensive borehole information is sometimes indispensable, geophysical data can in many cases suffice or provide continuous data extrapolated from or in-between a limited number of boreholes. Sites with permafrost are often remote, and this is also one of the main reasons why geophysical methods are used instead of the logistically demanding and expensive work needed to drill.

1.6.1 Electrical resistivity

Electrical resistivity increases substantially below the freezing point, this is due to the phase change from the electrically conductive water to non-conductive ice (Reynolds, 2011). Therefore this material property is well suited to study when the geophysical target of interest is permafrost.

The resistivity values of both frozen and non-frozen materials depend much on grain size, pore size, water content, degree of saturation, salinity and temperature (Kneisel et al., 2008). Thus the electrical resistivities of frozen sediments vary to a large degree depending on these parameters. Conspicuously low values of permafrost resistivity can be found in maritime sediments, where the presence of saline pore water raises the conductivity substantially. Values of resistivities in mountain permafrost settings however can be several orders of magnitude higher. Some resistivities of common materials and frozen sediments are presented in table 1 below.

The use of electrical resistivity tomography (ERT) in mountain permafrost research is widespread (E.g. Kneisel et al., 2000; Hauck et al., 2004; Isaksen et al., 2002; Etzelmuller et al., 2006), but it has also been used in lowland periglacial landform studies outside the mountain environment. Pingo ice content and internal structure was investigated in Alaska by Yoshikawa et al. (2006), and in Svalbard by Ross et al. (2007). Kristensen et al. (2011) examined the structure and composition of a tidewater push-moraine, Svalbard. Sass et al. (2010) analyzed the internal structure of European alpine mires (without permafrost) with ERT and compared with traditional methods (physical probing and coring) and ground penetrating radar (GPR).

In Yukon, Canada, Lewkowicz et al. (2011) examined palsa thickness in the discontinuous permafrost zone with the use of ERT. This is, to the best of the author's knowledge, the only recently published example of palsa permafrost depth determination with the use of 2-dimensional ERT. Earlier studies using 1-dimensional soundings on palsas include the study by Allard et al. (1986) by the Sheldrake River area, Québec, Canada, for permafrost thickness with the use of

1-dimensional resistivity soundings. Allard found an approximate ratio of palsa size to a little more than 1/3 of permafrost thickness.

Material	Resistivity range (Ωm)
Clay	1 – 100
Sand	100 – 5 x 10^3
Granite	5 x 10^3 – 10^6
Gneiss	100 – 10^3
Peat, Alps[a]	200 – 300
Groundwater	10 – 300
Permafrost, Alps	2 – 6 x 10^5
Rock glaciers	5 x 10^3 – 5 x 10^5
Frozen diamicton, Petuniabukta Svalbard	7 – 15000
Unfrozen diamicton, Petuniabukta Svalbard	130 – 1200
Pingo ice above marine limit, Adventdalen Svalbard	1 – 3 x 10^4
Pingo ice below marine limit, Adventdalen Svalbard	< 2000
Permafrost in the beachzone, Alaska	< 50
Glacier ice	10^6 – 10^8
Air	infinite

Table 1: Typical electrical resistivities of common unfrozen and frozen materials (From Hauck and Kneisel 2008; Kristensen et al. 2009 and references therein; [a]Sass et al. 2010).

2 METHODS

To determine depth of the permafrost in palsas and the excess ice fraction (EIF), electrical resistivity tomography (ERT), and permafrost table probing was used. Inclination was measured between each electrode to reconstruct the altitude variation over the measured transects. The measured resistivity was then modeled to acquire images describing the near-truth of the sub-surface.

2.1 RESISTIVITY THEORY

An overview of the theory of the electrical resistivity method is given in e.g. Reynolds (2011), Hauck and Kneisel (2008), and Loke (2001). Ohm's law is the fundamental equation describing the flow of electrical current in the ground. It can be applied in most geophysical cases, except where the current densities are so high that the linearity of the law might not apply (Reynolds, 2011). The equations apply to continuous direct-current (DC) flow, but they may also represent the effects of very low frequency alternating-currents (AC), when the effects of induction and displacement currents can be neglected (E.g. Stummer, 2003). Ohm's law in vector form is given as

$$\vec{J} = \sigma \vec{E} \tag{2}$$

where σ is the conductivity of the medium, J is the current density vector and E is the electrical field intensity vector. Most commonly the resistivity (ρ), the reciprocal of conductivity ($\rho = 1/\sigma$), is used in field applications. And electrical field potential, not electrical field intensity, is measured in the field. The relationship between the two is as follows below.

$$\vec{E} = -\nabla \Phi \tag{3}$$

where Φ is the electric potential, and ∇ is its variation in space

$$\frac{\delta}{\delta x} + \frac{\delta}{\delta y} + \frac{\delta}{\delta z} \tag{4}$$

Combining equation 2 and 3 gives

$$\vec{J} = -\sigma \nabla \Phi \tag{5}$$

Since the field installation of current electrodes is placed in the ground as point

sources, the relationship between current density and the current is given by the formula below (Dey and Morrison, 1979).

$$\nabla \cdot J = \left(\frac{I}{\Delta V}\right)\delta(x-x_s)\delta(y-y_s)\delta(z-z_s) \tag{6}$$

Where ΔV is the elemental volume surrounding the source of current I, and where x_s, y_s, z_s, define the point of injected electrical charge. And δ is the Dirac delta function.

The basic formula for the potential distribution due to a point current source can now be formed by rewriting equation 5 and 6 to

$$-\nabla \cdot [\sigma(x,y,z)\nabla\phi(x,y,z)] = \left(\frac{I}{\Delta V}\right)\delta(x-x_s)\delta(y-y_s)\delta(z-z_s) \tag{7}$$

Potential distribution in the ground due to a single point source of current is described by this formula (Dey and Morrison, 1979). Solving this problem is called 'forward modeling', which describes how to determine what potential distribution would be measured for a given resistivity distribution (i.e. geology, structure etc.) in the sub-surface (Loke, 2001). Using observed data to model the electrical potential distribution in the sub-surface is called inverse modeling. The inverse modeling is more complex than the forward problem, and will only be described briefly later.

Most applied direct-current (DC) electrical field survey methods are based on a measured potential difference between two potential electrodes (ΔU) placed on the surface, and two current electrodes where current is injected into the ground (I), with a known geometric factor (k), which depends on the arrangement of the electrodes. This gives a value of the apparent resistivity (ρ_a) of the ground sub-surface according to the equations below.

$$\rho_a = k\frac{\Delta U}{I} \tag{8}$$

where

$$k = \frac{2\pi}{\frac{1}{(r_{C1P1})} - \frac{1}{(r_{C2P1})} - \frac{1}{(r_{C1P2})} + \frac{1}{(r_{C2P2})}} \tag{9}$$

True resistivity is a material property, and is geologically diagnosticable. But measured resistance is dependent on the physical dimensions of the material, in

its simplest form; its cross-sectional area (A) and length (l). Therefore the geometry is needed to convert measured resistance to resistivity. The relationship between resistance (R), resistivity (ρ) and conductivity (σ) is given in the formula below.

$$\rho = \frac{1}{\sigma} = \frac{RA}{l} \tag{10}$$

To address the geometry of measured resistances between electrodes in the survey line, the geometric factor (k) (Equation 9) is used. Where r_{capb} is the distance between current electrode a and potential electrode b. The apparent resistivity (ρ_a) is then calculated by

$$\rho_a = k R \tag{11}$$

This measured resistivity is called 'apparent', since the current travels sub-surface within a medium that is, in almost all practical cases, anisotropic and heterogeneous. This means that each measured apparent resistivity value represents the resistivity for the whole current travel-path through a diverse resistivity distribution within the measured half-space. True resistivity values have a complex and, at the time of measurement, unknown distribution in the sub-surface. The distribution of true resistivity in a heterogeneous and anisotropic subsurface is only acquired after modeling of the observed data.

2.1.1 Measurement configuration and arrays

There are a range of standardized geometric arrangements of electrodes (arrays), which have their respective advantages and disadvantages. Some of the most commonly used array configurations are shown in figure 5.

Resistivity surveys can be performed by using a 'traditional' one-dimensional configuration, where the electrodes are moved manually between each measurement. When vertical changes are of interest for the investigation a vertical electrical sounding (VES) is carried out, which is done by moving the outer current electrodes of the Schlumberger array further out while the potential electrodes remain fixed. When lateral changes are of interest a constant separation traversing (CST) using the Wenner array, with fixed electrode spacing, is more suitable. During CST all electrodes are moved laterally along a transect for each measurement.

Both VES and CST profiling have clear limitations due to the work effort needed to move the electrodes between measurements and the limited one-dimensional data acquired, which can be hard to interpret.

An option to reduce these limitations is to use two-dimensional electrical resistivity tomography (ERT), which yields a much more accurate model of the sub-surface than the one-dimensional approach. In ERT a multi-electrode system collects information from combining multiple resistivity measurements with varying electrode spacing along the survey line. The array configurations used in VES and CST surveys are also commonly used in ERT surveys.

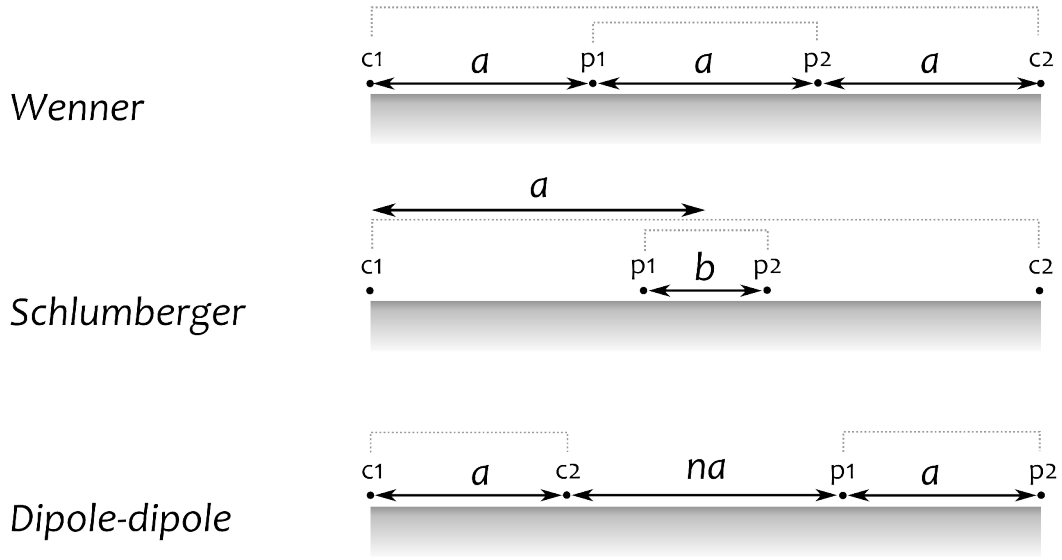

Figure 5: Some common types of arrays, where a and b are distances that describe the geometric factor, c1 and c2 are the current electrodes, and p1 and p2 are the potential electrodes. Extensively redrawn from Reynolds (2007).

2.1.2 Inversion

The goal during inversion of geophysical data is to find a model which fits the observed data, within reasonable limits. A synthetic dataset is created as a response to the estimated model parameters, from the known mathematical relationships, and is compared to the measured dataset. The goal is to make the difference between the measured and synthetic dataset as small as possible. This difference, the "degree of misfit", between the synthetic and measured dataset is expressed in percentage RMS error (Root Mean Square), and the process is repeated over a number of iterations to reach an acceptable value of this error (Reynolds, 2011; Loke, 2010).

Inversion modeling was done in RES2DINV v.3.59.64 by Geotomo Software. The inversion routine for RES2DINV is based on the smoothness-constrained least-squares method, which is based on the following equations.

$$(\boldsymbol{J}^T \boldsymbol{J} + u\boldsymbol{F})\vec{d} = \boldsymbol{J}^T \vec{g} \quad (12)$$

$$\boldsymbol{F} = f_x f_x^T + f_z f_z^T \quad (13)$$

Where f_x is the horizontal flatness filter, f_z is the vertical flatness filter, $\boldsymbol{J}$ is the Jacobian matrix of partial derivatives which describes the change in model response to a change in the model parameters, u is dampening factor, d is the model perturbation vector, and g is discrepancy vector (Loke, 2010).

2.2 SURVEY & PROCESSING

Five profiles were measured for electrical resistivity to determine depth to the base of permafrost, and to investigate the internal structure of the palsas. The survey was conducted between the 21st and 25th of August in 2012. Field weather observations are presented in appendix III.

Topography was measured with clinometer, and active layer depth was measured by probing during ERT data acquisition. Additionally, the vegetation was documented by photography at every electrode position on profile TA-196, and at every other electrode on TA-204. The measured profiles are between 40 – 560 meters in length, with electrode spacing between 0,5 – 4 meters with the aim to capture both finer details in the near-surface and resistivity changes at depth. Different sizes of palsas were chosen to be included in the survey to include both smaller mounds less than 1 meter and larger mounds up to 4 meters in height (Table 2 and Figure 6).

Profile	N	E	Azimuth [°]	l [m]	e [m]	σ^2
TA-196	N68°27.7498'	E020°54.1715'	10	240	2	1,31
TA-196EX	N68°27.7280'	E020°54.1347'	13	304	4	0,78
TA-204	N68°27.5832'	E020°54.1708'	280	560	4	0,51
TA-221	N68°27.7085'	E020°53.9660'	118	160	2	0,17
TA-316	N68°27.7729'	E020°54.2726'	135	40	0,5	1,31

Table 2: ERT survey transects. N and E are coordinates of the first electrode of the profile, azimuth shows profile direction from first electrode, l is the length of the profile, e is electrode spacing and σ^2 is the topography variance.

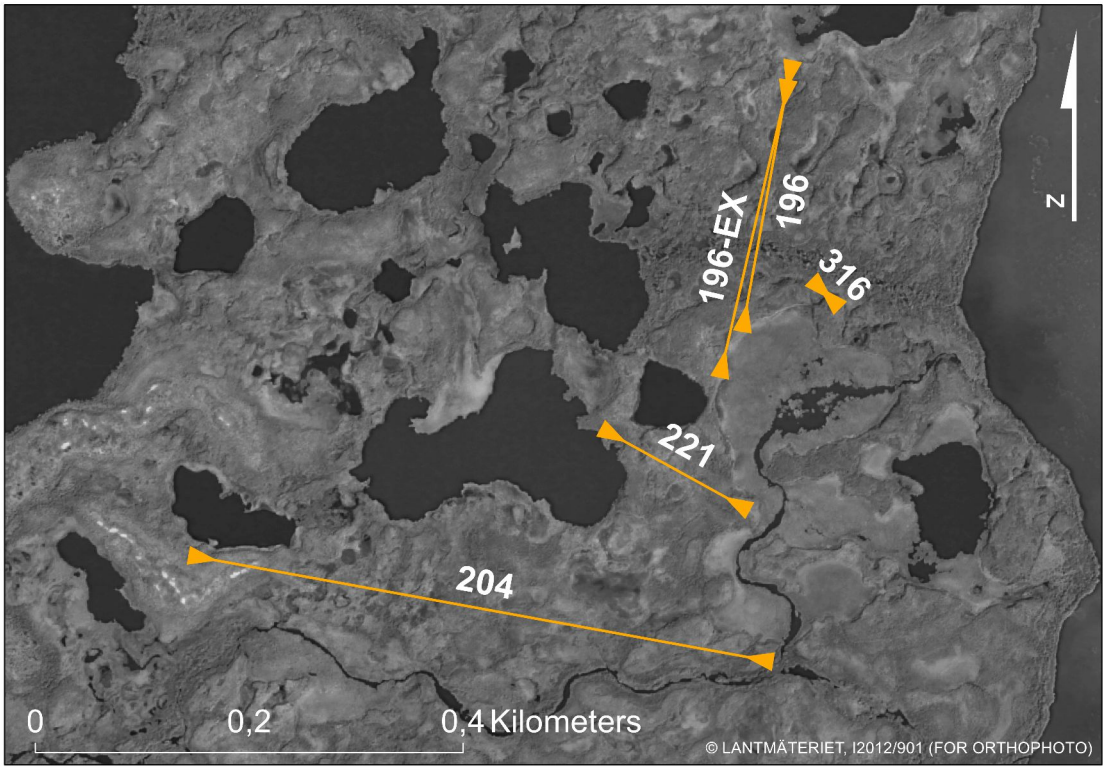

Figure 6: Location of ERT survey transects. Details of the profiles are described in table 2.

2.2.1 *ERT Profiling*

A Lund Terrameter multi-electrode imaging system from ABEM, Sweden, was used for the electrical resistivity measurements. The system consist of the Terrameter LS unit, 4 cable rolls with 5 meters maximum electrode spacing intervals, 2 cable joints, 84 cable-to-electrode jumper cables, 81 steel electrodes, and a 12 V / 75 Ah car battery.

The survey is performed by first placing the electrodes into the ground in the profile direction, with the desired electrode spacing, 21 electrodes are connected to each cable roll, with the 21st electrode connected to the first electrode of the following roll. The Terrameter LS unit is connected to the survey line at each cable joint location where measurements are performed in sequence shown in figure 7. When longer ('roll-along') surveys are performed, the first cable roll is moved to the front of the setup at the same time as the Terrameter is moved to the next cable joint position, before each sequence of measurements.

All ERT survey lines were measured using the Wenner configuration. Wenner array has the advantage of a high signal-to-noise ratio, compared to other arrays (Loke, 2010), and is favorable for depicting horizontal, or nearly horizontal, sub-surface structures/features (Reynolds, 2011).

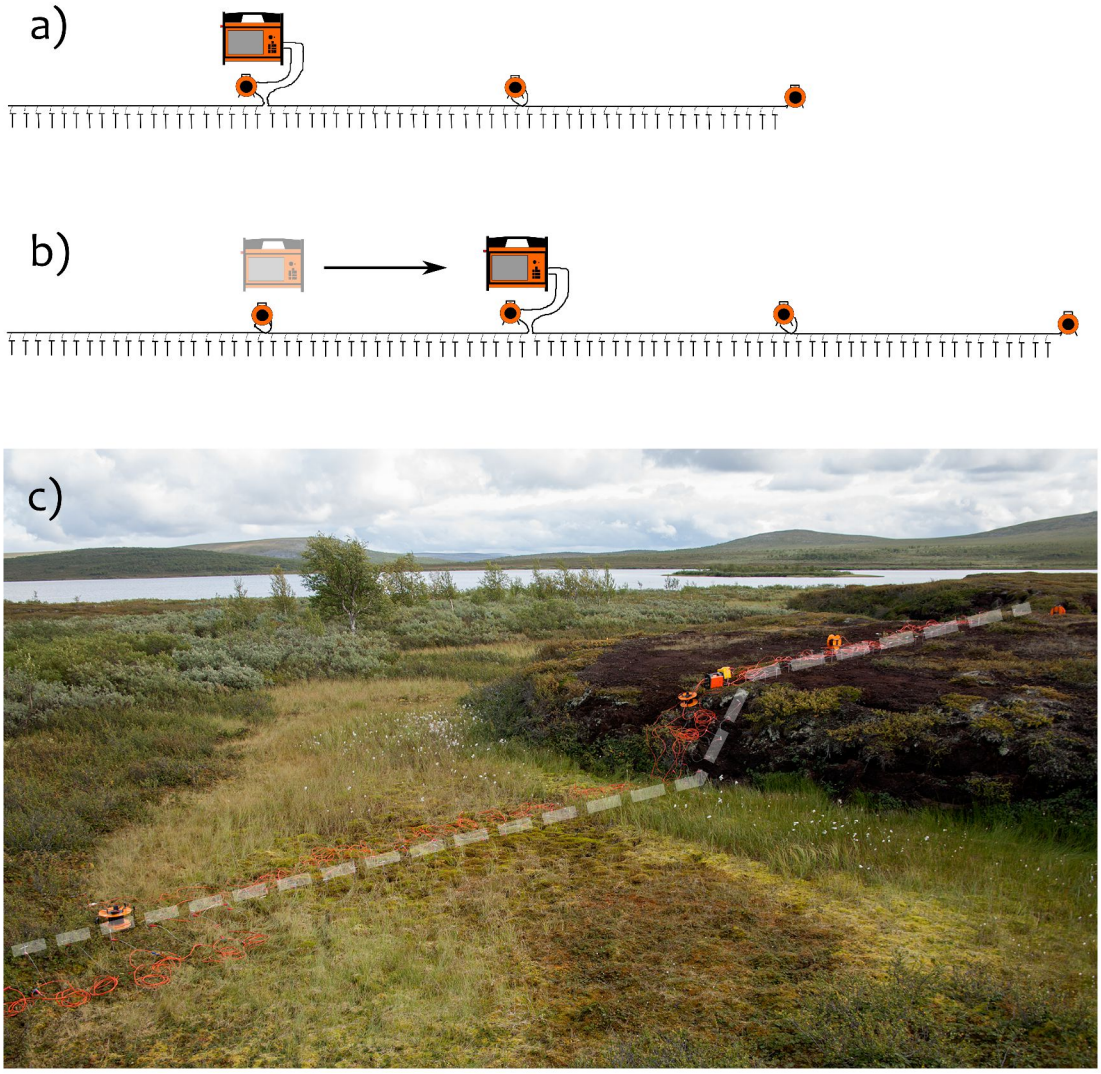

Figure 7: ERT profiling. a) First station in roll-along survey, with Terrameter connected between roll 1 and 2. b) Second station setup, with all four cables connected. c) Field setup. a) and b) are modified from Terrameter Inst., (2012).

2.2.2 *Topography*

All ERT profiles were measured with a handheld clinometer between each electrode to reconstruct the topography along the survey lines to be included in the inversion. The angles between each electrode was converted to an altitude of the electrode (h) at electrode position e according to the formula below,

$$h_e = h_{e-1} + [d \cdot \sin(a)] \tag{14}$$

where $h_{e\text{-}1}$ is the previous electrode altitude, d is the electrode spacing and a is

the measured angle, in degrees, between electrode *e-1* an *e* (Figure 8). Manual adjustments to the elevations had to be made after calculations to correct for the fact that measurement errors also accumulate during the summation procedure. Altitude for the first electrode was arbitrarily set at 550 meters (Mean altitude of Tavvavuoma) for all survey lines.

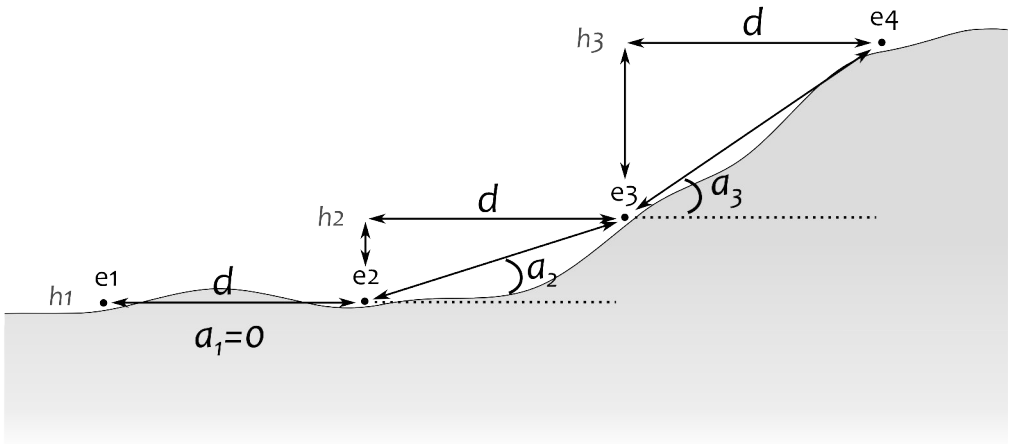

Figure 8: Topography reconstruction. Abbrevations are explained in the text.

For determining the height of each individual palsa DGPS readings from GPR surveys (Ylva Sjöberg, unpublished data) were used due to the higher accuracy required of these measurements. An average of five GPS samples on the top of each palsa were used for determining the top elevation, and a base elevation was determined by using data from several samples on the flat non-frozen mire surface.

2.2.3 Active layer

The resistivity profiles were probed at each electrode position with a 98 cm steel rod to determine the thawed layer depth where possible. Since the measurements were conducted in the late summer month of august, this depth measure represents the active layer depth.

The active layer probings are used to subtract the unfrozen surface layer depth from the depth to the base of permafrost in order to determine the thickness of the permanently frozen core of the palsas.

2.2.4 Inversion

The data files used for inversion are exported from the raw-data using the project files from the Terrameter LS unit. All ERT profiles were checked for any data quality inconsistencies, and electrode positions with abnormally high electrode contact resistances were filtered out before further processing. All profiles were topographically corrected before the inversion.

The inversion modeling was run using the Gauss-Newton method where the Jacobian matrix is recalculated after every iteration, thus is more time consuming but gives significantly better results than the faster quasi-Newton optimization technique when high resistivity gradients are expected (Loke and Dahlin, 2002). High resistivity contrasts are highly expected here, since the wet unfrozen mire is very conductive and permafrost consisting to a large part of ice is very resistive. The program was set to stop the inversion process after 5 iterations.

The optimal inversion modeling settings for each resistivity transect was determined by examining the model uncertainty for each inversion run. Four variations of inversion parameters were tested, which are listed below.

1. *Standard setting*. No changes from program start-up settings, standard least-squares constraints (l_2-norm) and normal mesh size.
2. *Robust setting*. Here the robust constraints for sharp boundary inversion (l_1-norm) was enabled at standard cut-off factors. All other settings are the same as previous. The robust constraints normally give higher accuracy where the geology consists of bodies separated by sharp boundaries.
3. *Robust setting with finest mesh size*. The type of mesh for the forward modeling sub-routine was set to finest setting. All other setting are the same as previous. The mesh setting defines the density of model blocks for the forward modeling sub-routine, and a finer setting normally increase the accuracy of the results at the expense of computation time.
4. *Robust setting with reduced effect of side blocks.* The effect of side blocks on the inversion process was set to be reduced. This reduces the presence of very high or low resistivities on the edge of the model. All other settings are the same as previous.

Interpretations and calculated depth to the base of permafrost is based on the

model with the best fit according to the model uncertainty values from inversion runs using these different setting.

2.2.5 Interpretation of depth in resistivity models

The depth to resistivity interfaces in the best fit inverted 2d resistivity model was made by examining the largest gradient of resistivity (δR) with depth (δz) (Equation 15), from the maximum resistivity observed where permafrost is likely to be present and downwards.

$$\boldsymbol{max}\,\frac{\delta R}{\delta z} \tag{15}$$

To find the depth and its uncertainty, the resistivity gradient of the lower boundary was fitted to a normal (Gaussian) distribution (Equation 16), where σ is the standard deviation, and μ is the mean of the distribution and also its maximum, thus represents the maximum derivative (Equation 15) and the inferred depth.

$$f(x) = \frac{1}{\sigma\sqrt{2\pi}}\ \mathrm{e}^{-\frac{(x-\mu)^2}{2\sigma^2}} \tag{16}$$

The range of uncertainty of the depth interpretation is given as one standard deviation (σ) of the normal distribution. The electrical resistivity of permafrost was taken as a mean of 2 – 4 samples of the resistive anomaly in the inverted resistivity model.

3 Results

3.1 Inversion parameters

The choice of parameters for inversion modeling was determined according to the procedure described in section 2.2.4 for all resistivity profiles. The results of profile TA-196 will be presented here and the remaining profiles are presented in appendix I.

Using standard setting (Figure 9), model uncertainty is high and the resistivity model has smooth resistivity transitions. Uncertainty is highest in the area just below the near surface area, where we are most interested in finding information about the resistivity transitions. RMS error is 5,24 for this model.

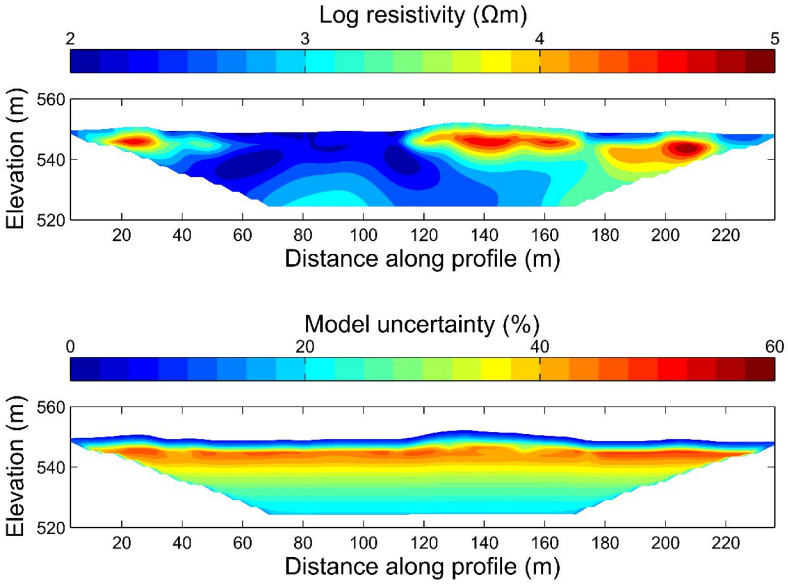

Figure 9: Inversion result for TA-196 with model uncertainty, standard setting.

Robust setting (Figure 10) gives sharper resistivity interfaces and much lower model uncertainty values, with an RMS error of 1,93. The highest uncertainty in this model is below blocks of high resistivity.

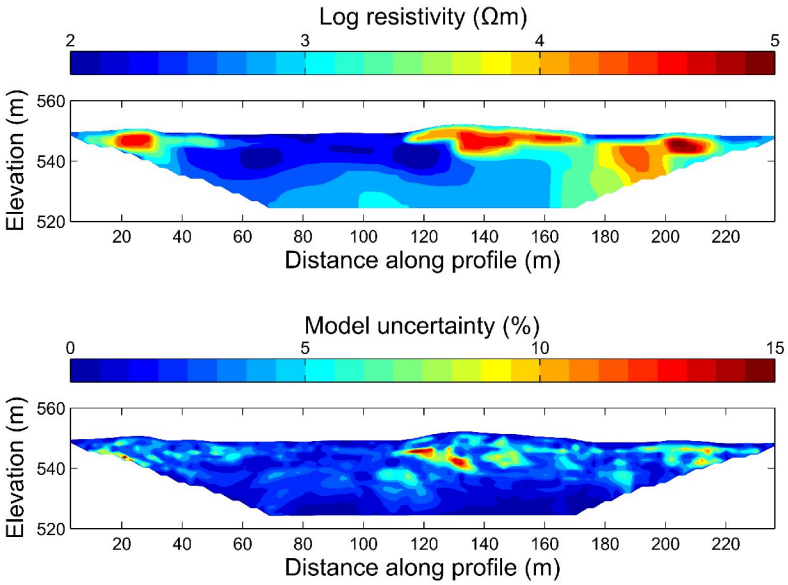

Figure 10: Inversion result for TA-196 with model uncertainty, robust setting. (Note the change in scale limits of the model uncertainty plot from previous figure)

Robust setting with finest mesh (Figure 11) produces a model with lower model uncertainty values than the using normal mesh. RMS error is 1,68 for this model. The areas of highest uncertainty are below blocks of high resistivity as the previous setting.

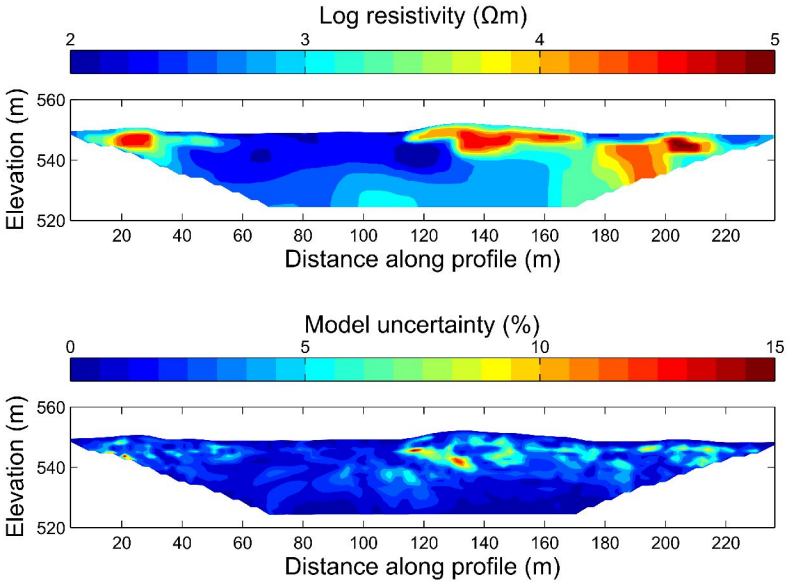

Figure 11: Inversion result for TA-196 with model uncertainty, robust setting with finest mesh.

Robust setting with the finest mesh and reduced effect of side blocks (Figure 12) produced a model with higher uncertainty values than without the side-block-effect-reduction enabled. The model has the highest uncertainty of all the robust inversion models, with an RMS error of 4,14.

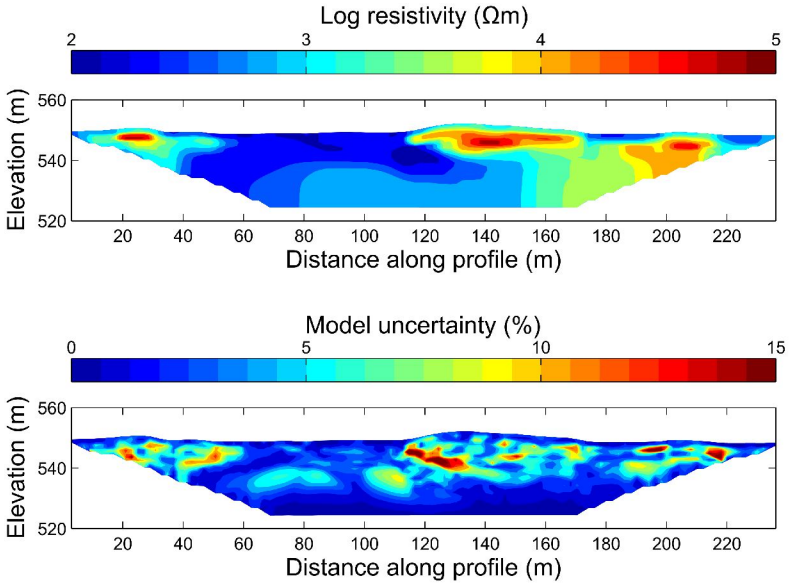

Figure 12: Inversion result for TA-196 with model uncertainty, robust setting with finest mesh and reduced effect of side blocks.

Of the four tested parameter combinations, the model with robust setting with the finest mesh size and without reduced effect of side blocks has the best fit for TA-196 and will be used for interpretation. Results from the other robust setting models also produced results with sufficient quality, but the standard least-squares constrained model did not. Since the measured target is known to have sharp boundary interfaces the robust setting is preferred in this case.

The remaining four profiles follow a similar pattern and are presented in appendix I. The only model that deviates from similar results as the presented profile is TA-204 where the robust constrained model with the effect of side block reduction enabled produced the best fit.

3.2 ERT Profiles

Here the result of each measured profile is presented together with a short description of the studied palsas. In appendix II the inverse models including the synthetic- and measured apparent resistivity plots are found for comparison. Though the inferred depths are presented with one decimal, it should be noted that the uncertainty of the method in most cases only allows

for meter scale accuracy at the most. Geographic location of all the profiles is found in figure 6.

3.2.1 TA-196

The first profile is 240 m long, is measured with electrode spacing of 2 m using the Wenner protocol and stretches over three palsas (TA-196-1;2;3). Between 60 – 110 m into the profile is a large wet fen area with a ≈ 1 m wide stream running through with some sedges (*S. lapponum*) and birches (*B. pubescens* ssp. *czerepanovii)* on its edges. The ends of the profile are wet/moist with no apparent permafrost present and should easily be penetrable with the ERT. The RMS error of the inversion model is 1,68 %.

TA-196-1 is part of a larger palsa-complex where several instrumented boreholes are placed in one end. Its top is located at 26 m from the first electrode and the palsa raises 1,7 m above the mire. The palsa has little or no apparent wind erosion on top. One borehole about 70 – 80 meters away, on the palsa complex show mineral contact at approximately 2 m depth (Ivanova et al., 2011).

The ERT profile starts 20 – 30 m from the palsa, and thus the penetration depth is not very deep under the palsa, and results are uncertain. The depth to the base of permafrost is inferred by fitting the derivative of the resistivity transition to a Gaussian distribution, described in method section, giving a maximum at 6,4 m depth with a standard deviation of 0,9, representing a ± 0,9 m uncertainty (Figure 13). A shallower interface is also visible at ≈ 2 m depth.

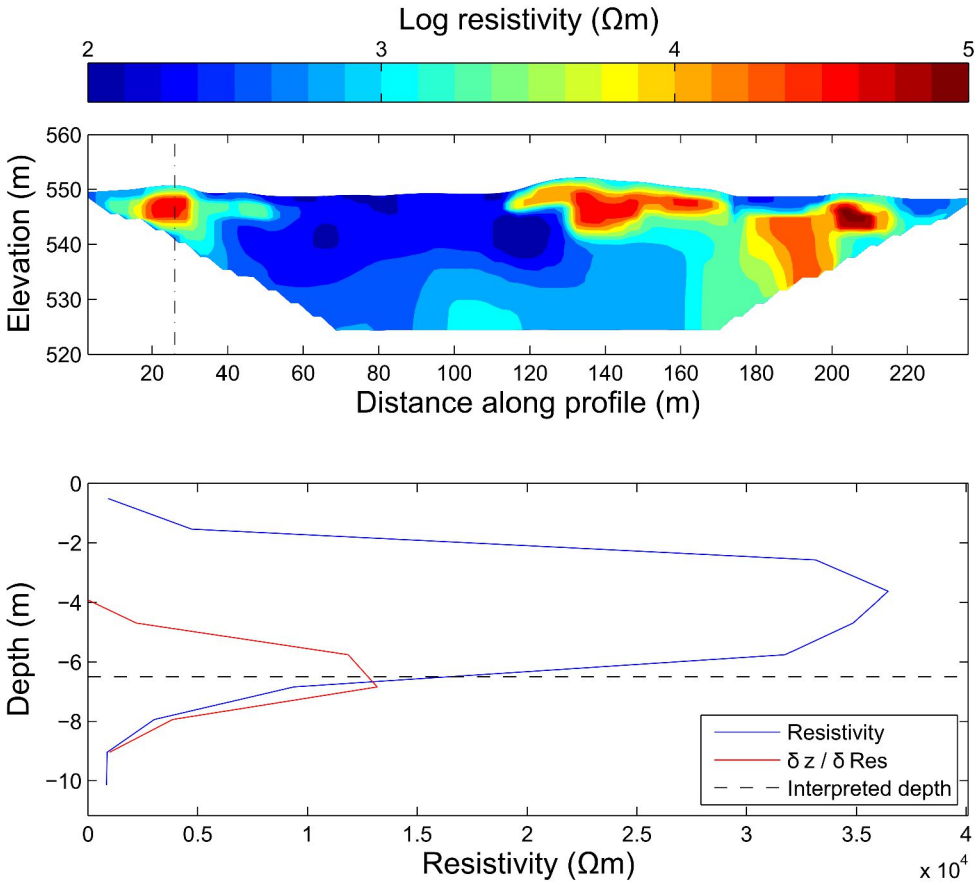

Figure 13: Palsa TA-196-1. a) Resistivity model with dashed line indicating location of palsa. b) Vertical plot of model resistivity at palsa location. Dashed line indicating interpreted depth to the base of permafrost.

TA-196-2 is in the middle of the transect at 136 m from first electrode and is the highest palsa of the studied area at 4,0 m above the mire surface. The palsa is dome-shaped, and circular to oval in area. Wind erosion is visible on the southern flank, while the northern flank is covered with relatively dense but low vegetation of *B. nana* and more.

Since the palsa is located in the middle of the ERT transect the penetration depth is good. Depth to the base of permafrost is inferred to 7,6 m with standard deviation of 1 m (Figure 14). A first interface is also visible at 2 – 3 m depth.

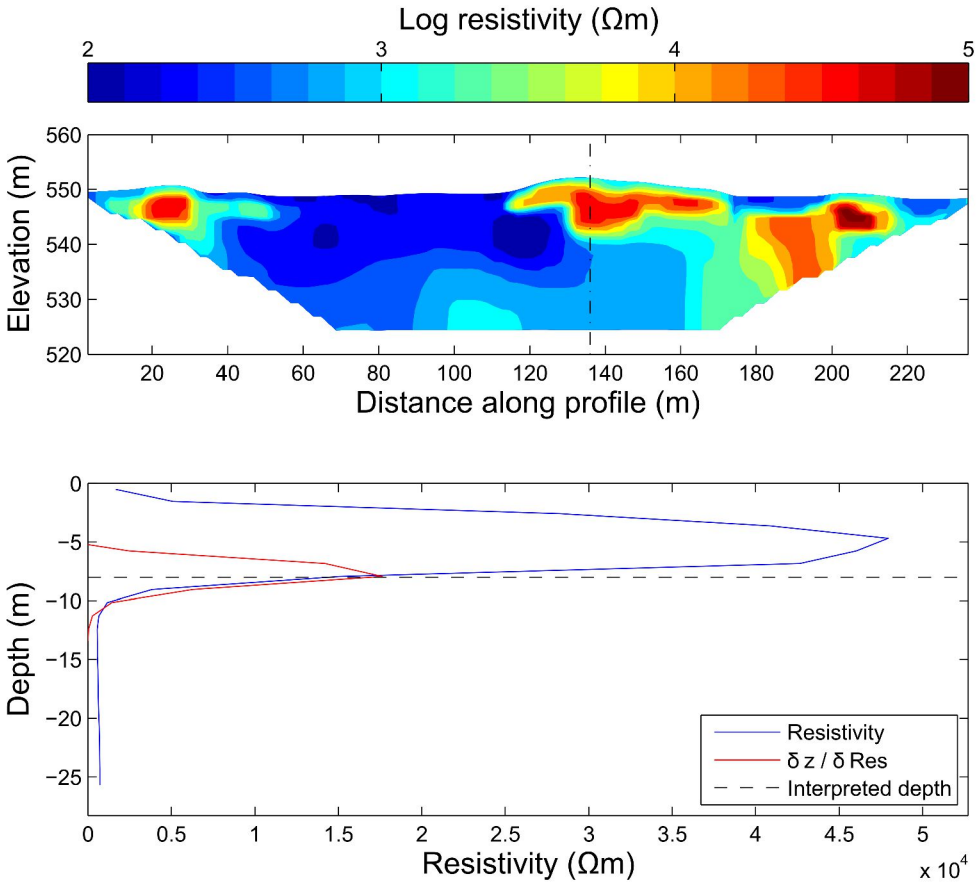

Figure 14: Palsa TA-196-2. a) Resistivity model with dashed line indicating location of palsa. b) Vertical plot of model resistivity at palsa location. Dashed line indicating interpreted depth to the base of permafrost.

TA-196-3 is located at 204 m from the first electrode and raises 1,5 m above the mire surface. The palsa is of plateau type and is connected to the dome-shaped 196-2, with a thaw pool separating the two along the transect. The surface is covered with low vegetation, with no signs of erosion on the top surface. Depth to the base of permafrost is inferred to 6,7 m with a standard deviation of 1,2 m (Figure 15).

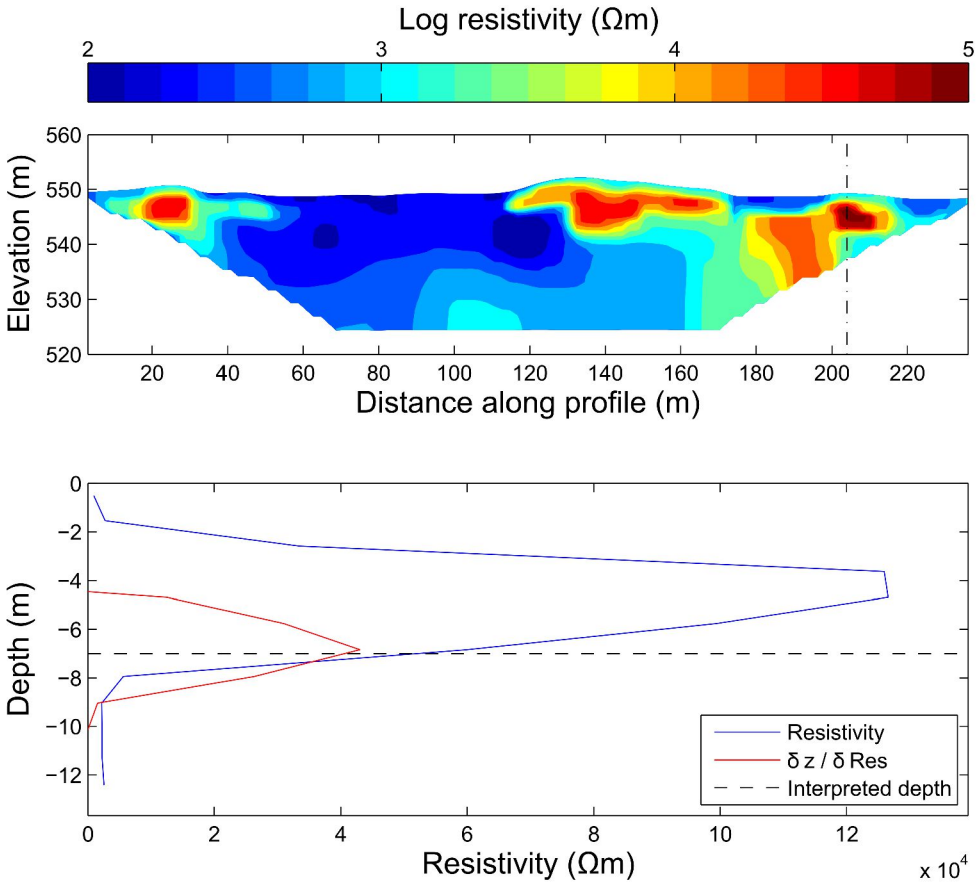

Figure 15: Palsa TA-196-3. a) Resistivity model with dashed line indicating location of palsa. b) Vertical plot of model resistivity at palsa location. Dashed line indicating interpreted depth to the base of permafrost.

3.2.2 TA-196EX

This profile is an extended version of profile TA-196 using the Wenner protocol with 4 m electrode spacing and with the first electrode location moved 50 m in approximately south direction and the last electrode moved approximately 20 m in northerly direction from its original location. The aim to measure the same profile with wider electrode spacing was to get more data coverage and enable further penetration depth below the highest palsa, TA-196-2, and thus, hopefully, acquire a more reliable depth estimate. The percentage RMS for the inverted model is 1,66. Figure 16 shows the location of the three palsas covered by the profile.

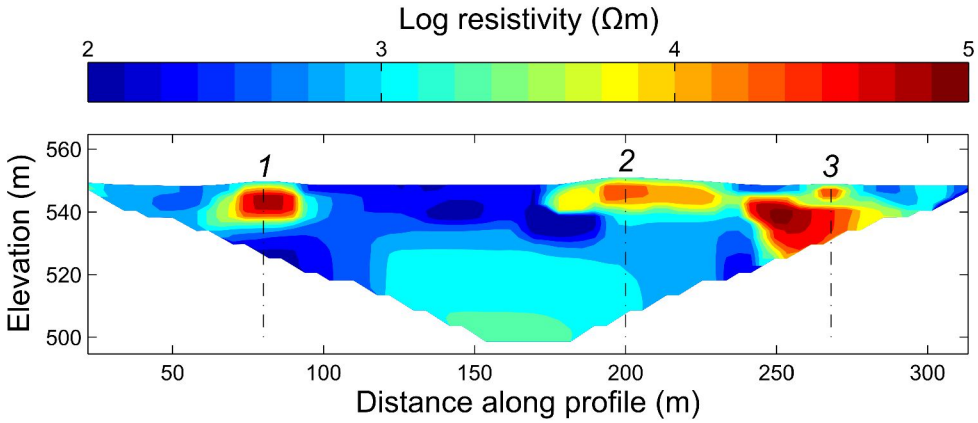

Figure 16: Profile TA-196EX with location of palsas indicated, 1) TA-196EX-1, 2) TA-196EX-2 etc.

Palsa TA-196-1 shows an interface to the base of permafrost at 11,0 meters (σ = 1,8 m) (Figure 17). This is ≈ 5 m deeper than the results from the TA-196 profile. This depth should be a better estimate of the true depth since the previous transect crossed this palsa in the beginning of the profile, thus the penetration depth was much shallower.

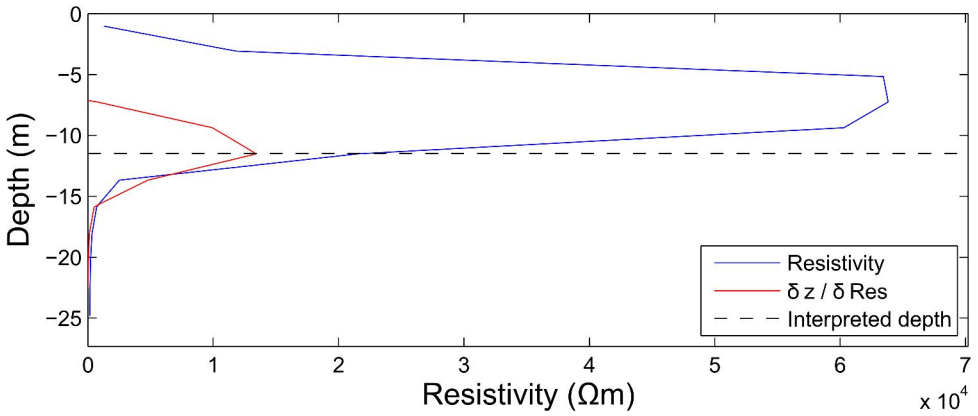

Figure 17: Palsa TA-196EX-1. Vertical plot of model resistivity at palsa location. Dashed line indicating interpreted depth to the base of permafrost.

For palsa TA-196-2, the results are very similar to the previous transect with the 2 m spacing. The depth is inferred also here to 7,6 m with slightly higher uncertainty at σ = 2,2 m.

TA-196EX-3 is underlain by a deeper high resistivity anomaly stretching from underneath the fen to the south of the palsa (See figure 16). This might possibly be an inversion artefact, or it could indicate a high resistivity body at depth. The

permafrost body of the palsa is interpreted as the isolated high resistivity block on top of the deeper body to 5,2 m. This data is however difficult to interpret, as few very data points represent the supposed frozen body of the palsa, and no Gaussian distribution could be fitted to the gradient (Figure 18).

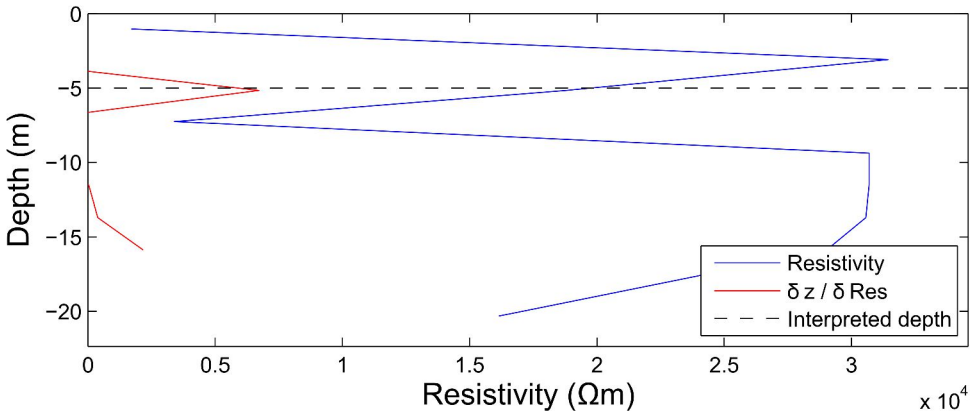

Figure 18: Palsa TA-196EX-3. Vertical plot of model resistivity at palsa location. Dashed line indicating interpreted depth to the base of permafrost.

A deeper resistivity interface under the middle of the fen could also be detected by the ERT, which could be a possible bedrock interface, at approximately 16 m depth with about ± 4 m uncertainty.

3.2.3 TA-204

TA-204 is the longest measured profile for the survey at 540 m, with an electrode spacing of 4 m using the Wenner protocol. The survey line crosses 11 permafrost mounds of mostly plateau character (TA-204-1;...;11) (Figure 19) with consistently low elevations (< 1,5 m) and commonly also large areal coverage in the eastern end. Towards the western end the peat plateaus become increasingly more fractured into smaller string-shaped structures.

The middle part of the profile was seemingly drier than the rest and other profiles closer to the stream in the east. Vegetation on the top of palsas, notably *R. Chamaemorus,* was often at or near wilting point. This could also have been due to some disease of *R. chamaemorus*, but the author cannot make this judgement. Close to the western end of the profile an esker-like glaciofluvial deposit is exposed on the surface, which shows on the ERT model as an area of very high resistivity from the surface and downwards. This deposit was very dry, and could due to the draining capabilities of the material have been the cause of the dry conditions on and in-between the palsas. Two electrodes on top of the deposit were excluded in the modeling due to very high electrode contact

resistance. Percentage RMS error for the model is 3,14.

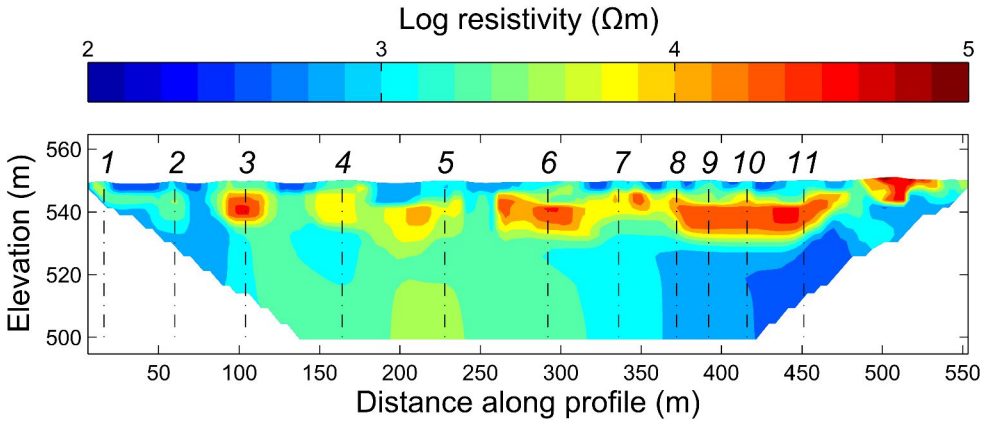

Figure 19: Profile TA-204 with location of palsas indicated, 1) TA-204-1, 2) TA-204-2 etc.

Palsa TA-204-1 is a low elongated peat plateau, with a flat top and with no visible signs of erosion where the profile crosses. It is not possible to derive depth to permafrost base with ERT, due to too shallow investigation depth, and there is also no DGPS data to extract an exact elevation for the mound. The fen between palsa 1 and 2 is situated close to a small stream, and is covered with *B. nana* and some *Salix* sp.

TA-204-2 is a low, oval-elongated flat-topped peat plateau, less than 1 m high. Dry vegetation covers the top of the mound, and no obvious signs of erosion are visible on the surface. Here the depth to base of permafrost could be inferred to 12,9 m (σ = 2,4 m).

TA-204-3 is a bit larger in areal coverage than the previous peat plateau, but has the same shape characteristics. The mound is 1,2 m high. The inferred depth to the base of permafrost is the same at 12,9 m (σ = 1,8).

TA-204-4 stretches about the same length as the previous mound under the ERT profile, is roughly the same size, but is not as distinctly bounded at the edges. The mound is 1,2 m high. Inferred depth of permafrost interface is at 15 m (σ = 1,6).

TA-204-5 is a flat-topped peat plateau, only about 0,5 m high. The depth to permafrost base is inferred to 15,2 m (σ = 3,7).

TA-204-6 is a flat-topped peat plateau, 1 m high. Small patches of living colonies of *Sphagnum* and other moss species are found on the top of the mound where the profile crosses. The depth to the base of permafrost is inferred to 14,1 m (σ = 3,5).

TA-204-7 is an elongated peat plateau or string-shaped palsa feature, 1,1 m high. The inferred depth to the base of permafrost is 11,5 m (σ = 2,3).

TA-204-8 is a string-shaped palsa lying perpendicular to the profile. The mound is about 1,2 m high. The inferred depth to the base of permafrost is 11,5 m using the maximum gradient, since the gradient could not be fitted to a Gaussian distribution. The mounds in this section of the profile are generally smaller and more debonded/clustered than the eastern end.

TA-204-9 is also a string-shaped mound, lying perpendicular to the profile, with a height of 1,3 m. The depth to the base of permafrost is inferred to 17,0 m (σ = 2,4).

TA-204-10 is a string-shaped palsa, 1,1 m high, lying perpendicular to the profile. Depth to the base of permafrost is inferred here to 17,7 m (σ = 2,3), which is the deepest resistive interface found. While the previous mounds have lacked distinct signs of erosion, this mound exhibits clear signs of block erosion on the western flank, into the thermokarst lake that is enclosed by the peat plateau. There is interestingly a sign of just as deep permafrost underneath this thermokarst lake as underneath the frozen mounds.

TA-204-11 is also a string-shaped palsa, 1,2 m high, but lying almost parallel to the ERT profile. Like TA-204-10, this palsa is experiencing block erosion into the pond on the eastern flank. Depth to the base of permafrost is inferred to 14,8 m (σ = 2,3).

The ERT profile crosses a ≈ 2 – 3 m high sedimentary ridge of glaciofluvial origin (Lagerbäck, 2012) in the western end. The depth of this feature is about 8,2 m with σ = 1,3, and with resistivities of 40000 – 80000 Ωms.

3.2.4 TA-221

Profile TA-221 starts right next to one of the larger lakes in the area and continues over palsas of plateau-type (TA-221-1;2) (Figure 20) south-eastward and ends before a small stream in the east. The profile is 160 m long and is measured with 2 m electrode spacing using the Wenner protocol. All of the mounds are interconnected within the peat plateau, but two topographic peaks along the profile were identified for the analysis. Between mound 221-1 and 221-2 the profile passes right next to a thaw depression which shows as an area of low resistivity separating the two resistive anomalies. Vegetation covers the surface without any sign of erosion. The resistivity model has an RMS error of 3,48 %.

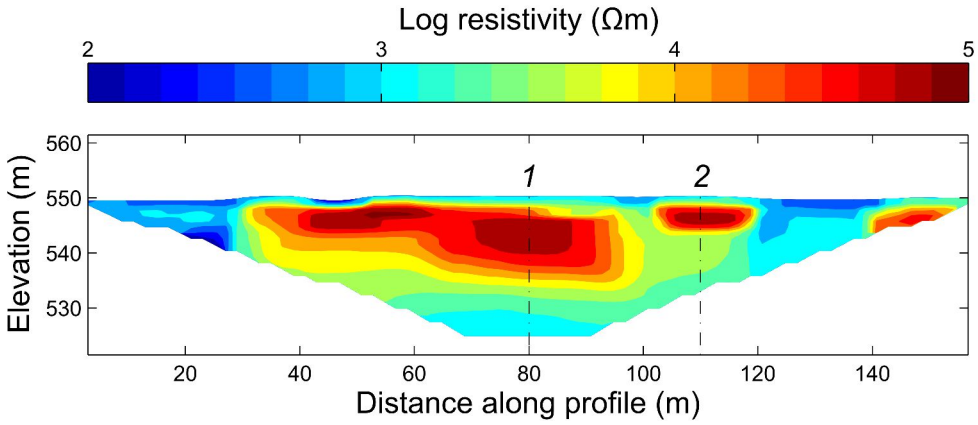

Figure 20: Profile TA-221 with location of palsas indicated, 1) TA-221-1, 2) TA-221-2.

Palsa TA-221-1 is a 1,8 m high mound, with some thaw depressions present on its surface. Depth to the base of permafrost under the top is inferred to 12,0 m. The modeled resistivity change is smooth, with standard deviation of 2,5 m (Figure 21).

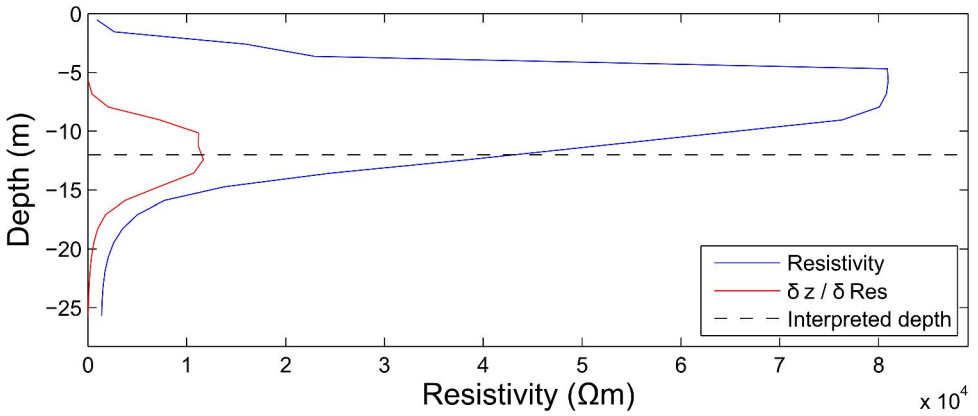

Figure 21: Palsa TA-221-1. Vertical plot of model resistivity at palsa location. Dashed line indicating interpreted depth to the base of permafrost.

Palsa TA-221-2 is part of the same palsa plateau complex as the previous mound but is isolated from the same along the ERT transect due to the presence of a thaw depression. This resistive anomaly has a shallower lower interface compared to TA-221-1, indicating permafrost base at 5,9 m depth (σ = 0,9).

3.2.5 TA-316

Profile TA-316 is measured over the edge of one single palsa (TA-316), it is only

40 m long, starting on the wet fen and ending close to the other end of the palsa. The profile is measured with 0,5 m electrode spacing using the Wenner protocol.

Palsa TA-316 is 2,2 meters high, almost circular in shape, and is part of the same palsa complex as 196-1. The top of the palsa is probably subjected to wind erosion since a large part of the vegetation is stripped off large areas of the top surface. The sides are subject to pronounced block erosion, where large blocks of peat (0,5 – 1,5 m) is tilted towards the wet pool that surrounds the palsa, many cracks also run along the palsa top surface.

The ERT profile was measured with 0,5 m electrode spacing to capture finer details of the active layer and the thawing edge. No depth could be inferred due to too shallow investigation depth. The resistivity of permafrost could be determined to 25000 – 45000 Ωm, with the high resistivities closer to the thawing edge and the lower values closer to the top (Figure 22).

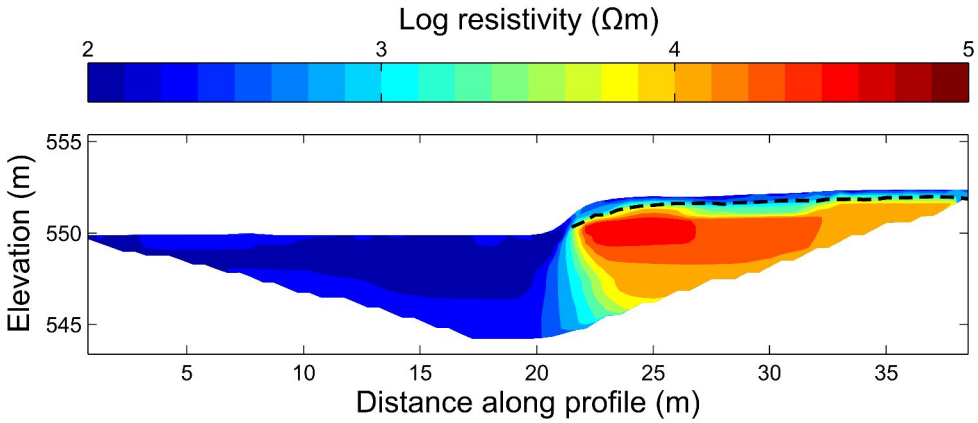

Figure 22: Profile TA-316 showing edge of palsa TA-316. Dashed line shows active layer probings.

3.3 SUMMARY

The table below (Table 3) summarize the results from the ERT survey, together with the physical probings of the active layer, the elevation of the mounds, permafrost resistivities, and the calculated excess ice fraction (EIF) for each mound.

Mound / Palsa #	x-location [m]	h [m]	Z_{PF} [m]	σ [m]	Z_a [m]	PF Resistivity [Ωm]	EIF
196-1	26	1,7	6,4	0,9	0,47	35000	0,28
196-2	136	4,0	7,6	1,0	0,63	46000	0,54
196-3	204	1,5	6,7	1,2	0,48	125000	0,23
196EX-1	80	1,7	11,0	1,8	0,47	62000	0,15
196EX-2	200	4,0	7,6	2,2	0,63	23000	0,54
196EX-3	268	1,5	5,2[a]	-	0,48	31000	0,33
204-1	15	-	-	-	-	-	-
204-2	59	0,7	12,9	2,4	> 0,98	3000	0,06[b]
204-3	103	1,2	12,9	1,8	0,47	31000	0,09
204-4	165	1,2	15,0	1,6	0,45	8000	0,08
204-5	228	0,5	15,2	3,7	> 0,98	5700	0,04[b]
204-6	290	1,0	14,1	3,5	0,68	32000	0,07
204-7	334	1,1	11,5	2,3	0,45	8500	0,09
204-8	371	1,2	11,5[a]	-	0,45	20000	0,09
204-9	393	1,3	17,0	2,4	0,46	27000	0,08
204-10	416	1,08	17,7	2,3	> 0,98	21000	0,06[b]
204-11	451	1,17	14,8	2,3	0,45	24000	0,08
221-1	80	1,8	12,0	2,5	0,48	80000	0,16
221-2	110	2,1	5,9	0,9	0,52	77000	0,38
316-1	34	2,2	-	-	0,62	25000 – 45000	-

Table 3: Summary of results from the ERT survey. x-location is the distance in meters from the first profile electrode, h is the height of palsa above surrounding topography, Z_{PF} is the depth to the permafrost base, σ is the standard deviation of depth (See method section), Z_a is the active layer depth. [a]Gaussian fit not possible, depth taken as max gradient. [b]Where the active layer was deeper than 0,98 cm it was set to 1 m to calculate the EIF.

4 Discussion and interpretation

4.1 Permafrost thickness from ERT

The results from the ERT survey show permafrost thickness ranging from 5 – 17 m under the surveyed mounds. This is in the approximate same range as results show from two previous studies known to the author using resistivity soundings conducted on several palsas. In the Yukon territory, Canada, Lewkowicz et al. (2011) found thicknesses in the range between 0,9 – 15 m with the use of ERT, and Allard et al. (1986) report thicknesses in the range of 3 – 18 m acquired from 1-dimensional resistivity soundings in Québec, Canada. No similar studies on palsas from Scandinavian locations are published. The deepest resistive anomalies (Interpreted as permafrost) were found in the west end of the study area, and it was a general shallower trend to the east. The reasons behind these differences and alternative interpretations will be discussed under headline 4.2 and 4.4.

The depth to permafrost base at palsa 196-2 was inferred to (exactly) 7,60 m on both ERT profiles crossing this palsa (TA-196 and TA-196EX). This is not to be confused with a centimeter accuracy of the results, but it does strengthen the probability of an accurate model of permafrost thickness under the palsa, to a range within the given uncertainty bounds. Physical validation is available from 196-2 in the form of a 10 m deep borehole on top of the palsa (Ivanova et al., 2011). The sediment log shows an interface to ice-bearing sediments at 2,8 m, and an interface from low to high resistivity is also visible on the ERT model as a maximum gradient at 2,6 m. This shows that the shallow geology is represented well by the resistivity model, with a few decimeters accuracy. Thermistors show cryotic conditions all the way down to the bottom of the borehole, at 10 m depth (-0,2°C) (Figure 23).

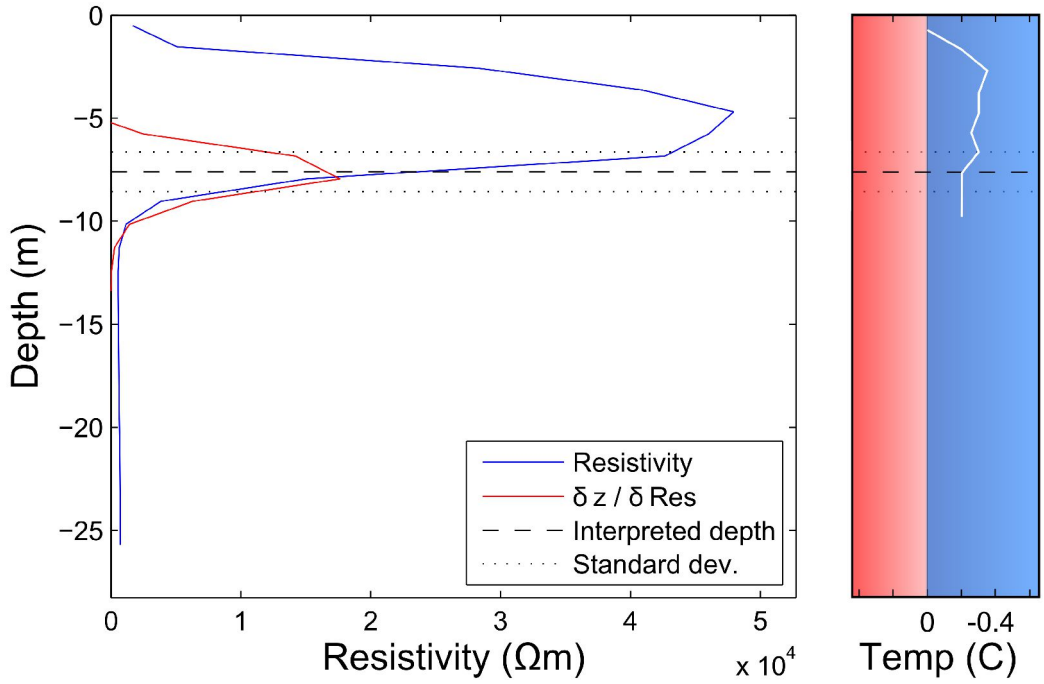

Figure 23: TA-196-2 resistivity model with borehole temperature (Temp. data redrawn from Rivkin, 2009).

This difference in depth of permafrost is greater than the stated uncertainty range of the modeled depth. Three explanations/hypotheses has been identified that could explain the deviation between the depth indicated by borehole to the modeled depth.

1. The base of permafrost under the palsa has undergone thawing from below during the time that has passed since the borehole temperatures were registered.
2. The bottom of the borehole has undergone freezing from above or below during the time passed since the borehole was drilled to the time the thermistors registered the temperatures.
3. The inverted model does not show an accurate fit of the real sub-surface conditions under the palsa.

The rate of thaw required to decrease the thickness of permafrost by a minimum of approximately 1,5 meters (10 - [7,60 + σ]) during the 4 year period since the borehole was drilled (2008-09-04) is very high. The probability of such thaw rate is however beyond the scope of this study, and would require

thermodynamical modeling, probably incorporating the flow of groundwater. Recent borehole temperature data that could verify such thaw rate is unfortunately not available, due to early failure of the thermistor cable (Britta Sannel, personal communication). Freezing of the borehole from above is probably unlikely as well. Minimum temperature of the day the borehole was drilled was 4,9°C (SMHI, internet), and persistent sub-zero temperatures were not reached the following month after this. The actual date when the temperature measurements were logged have not been acquired however. A likely scenario could be a combination of some minor basal thaw during the 4 year period, and a 'normal' error of the inversion model, i.e. within the uncertainty range of the method. Another possibility could be the expulsion of sub- or intra-permafrost water, similar to 'icings' or 'aufeis' formation (French, 2007), which filled the borehole with ice before temperatures were registered.

It must be noted that the complex 3d geology of a palsa bog is problematic when it comes to quantitatively interpreting depths from a single ERT profile measured in only 2 dimensions (Dahlin and Loke, 1998). It would likely not have generated the same permafrost interface depth if another transect were to be measured perpendicular to the mound, crossing its top. The electrical currents travel in a semi-circular half-space in the sub-surface, and thus also capture the electrical properties of surrounding material, not only directly below the studied object, this can lead to both under- and overestimation of the depth, depending on the circumstances. Also, the inversion resistivity model is not a unique fit to the sub-surface, which has to be taken into consideration. Small or large changes in the model can produce a forward modeled response that fits the measured apparent resistivity section just as well, and a low RMS error cannot truly predict the accuracy of the inverted model.

The electrode spacing is greater than the average active layer depth in most cases when the 2 and 4 m spacing are used. Due to this, the top of permafrost interface (active layer depth) is not shown in most of the ERT data. The frost table probings are used instead for this interface, and are in every case more accurate since they are direct measurements. The exception is profile TA-316 where 0,5 m spacing was used, which captures the active layer in the ERT in good agreement with the probings (Figure 22).

A first shallow interface at around 1 – 3 m depth shown in many of the resistivity sections is most probably the interface between peat and ice-rich sediments, not the active layer. For palsa 196-2 the borehole log (Ivanova et al., 2011) shows sediment interface at about 2 m, the same interface is visible in the resistivity model. A shallower hand-driven borehole (Ylva Sjöberg, unpublished data) about 45 meters into profile TA-221, in the middle of a small thaw depression, shows sediment interface at 1,55 m. The resistivity transition from

low to high in the model starts right at 1,55 m, though the maximum gradient is positioned deeper at about 2,50 m. This could mean that the sediments below the depression are thawed about one meter below the interface. The sharp increase in resistivity at and below sediment interface in most profiles could also support the assertion that excess ice is mainly formed in the sediments, and not as extensively in the peat (E.g. Kujala et al., 2008).

The 4 m electrode spacing profile TA-204 might not have captured the near-surface frozen conditions of mounds indicated by physical probings, possibly could this also be due to low contents of excess ice or warm permafrost. On TA-196EX however the frozen material close to the surface is visible. The scale also reveals other interesting sub-surface characteristics, such as a possible bedrock interface. The possible bedrock interface is under profile TA-196EX at 16 m (± 4 m). The resistivity values under this transition are in the range 1000 – 3000 Ωm, which falls conveniently between granite and gneiss (See table 1), which is likely to underlie the palsa bog (SGU, internet). This supports the interpretation that this is a bedrock interface. Deep resistive anomalies under profile TA-204 was also revealed by the 4 m electrode spacing, which are the deepest plausible permafrost depths (at up to 18 m depth) found during this survey, and will be discussed using the resistivity values of permafrost and excess ice content.

4.2 Excess ice and permafrost resistivity

Resistivities of permafrost vary substantially between $3x10^3$ – 10^5 Ωm, with an average around $4x10^4$ Ωm. These values might indicate warm permafrost in at least some of the palsas with lower resistivity values, since increase of water content in warm permafrost raise the conductivity. Warm permafrost here has been confirmed by Christiansen et al. (2010), from a borehole close to palsa TA-196-1. This also indicates that the permafrost resistivities, thus possibly also temperatures, despite the relatively small distances separating the palsas, vary a lot depending under the different conditions/environments in the bog which they exist.

Calculated EIF values varies between 0,04 – 0,58, with a mean of 0,19. The EIF's accuracy depends on an accurate depth estimate of the permafrost depth, which is undoubtedly the most uncertain quantity in the equation. One profile that particularly stands out is profile TA-204 where all palsas have EIF below 0,11, with a mean of 0,08. Excluding this profile and calculating the average EIF gives a mean of 0,34, which agrees well with Allard et al. (1986) mean EIF (0,37), and similar results are also given in Lewkowicz et al. (2011).

A closer look on the outlier profile TA-204 reveals that mean permafrost resistivities are less than half compared to the mean of the other profiles. Lower

resistivity values could be associated with warm permafrost, but also with a lower excess ice content, since a lower content of ice will raise the conductivity (E.g. Reynolds, 2011). Thus the EIF calculation appears credible. A significant variation of excess ice content in the permafrost within the area seems to be likely.

Along the same profile, a gradual increase in permafrost resistivities to the west is observed (Figure 24), and a similar increase in permafrost thickness is also visible in the model, though with high uncertainty in the west end. This observed increase in permafrost resistivities and increased depth to the west might be due to a change in-, and increased influence of the underlying sediments, from the sand/silt found in sediment cores in the eastern part of the study area (Ivanova et al., 2011), to a coarser glaciofluvial sediment, shown in outcrop at the western end of profile TA-204 (Figure 25), and which are indicated on the map of Quaternary deposits (Lagerbäck, 2012). Glaciofluvial deposits have a high hydraulic conductivity (E.g. Hendriks, 2010), thus drain easily and also hold less soil moisture above the groundwater level than silts and fine sands. This is evident where the sediment is in outcrop in the end of the profile, showing high resistivities of 40000 – 80000 Ωm indicating very dry conditions.

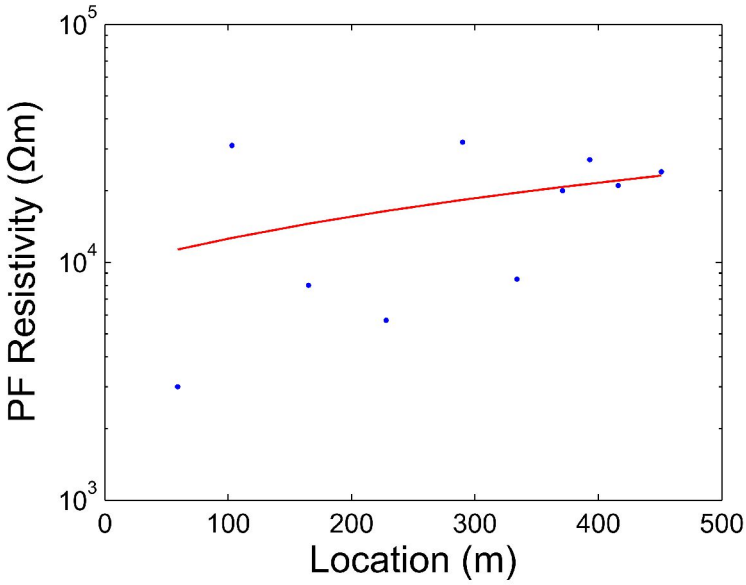

Figure 24: Permafrost resistivity along TA-204


Figure 25: Glaciofluvial deposit in outcrop, Profile TA-204 indicated by dashed line.

These coarse grained glaciofluvial deposits hypothesized to constitute the frozen core below mounds TA-204-8;11 are less frost susceptible and thus have less ability to form segregation ice than deposits of finer grain size such as silts and fine sands (French, 2007). Since higher amounts of energy are required to freeze frost susceptible sediment, due to latent heat release during the formation of segregation ice, permafrost will have the ability to aggrade deeper in non-frost susceptible sediments in a shorter amount of time. The ice content in this type of sediments would naturally be lower than in sandy/silty materials, since water mainly freeze *in situ* as pore ice (French, 2007). This can explain the presence of deep permafrost, and a low amount of excess ice in the sediments could explain the comparably low elevations of the mounds TA-204-8;11, despite the great thickness of permafrost.

4.3 Internal structure of palsas

The ERT models from profiles measured with 2 m and 0,5 m spacing reveal details about the internal structure of the palsas, while the 4 m spacing profiles mostly have too coarse resolution to show the internal variations with satisfactory details.

Some interesting features of palsa morphology under palsa TA-196-2 could be detected by the ERT. First, a zone of low resistivity under a string of high resistivity at the western flank indicates a non-frozen hollow (Figure 26). This suggests that the palsa might be thawing from the side and below, which could potentially result in the initiation of block erosion at the palsas western flank.

This can possibly also strengthen the probability that the previously proposed hypothesis that the palsa is thawing from below is accurate. However, no other measurements are available to support this. A similar string of high resistivity extends from palsa TA-196-1 in the direction of the small stream lying perpendicular to the profile (Figure 13). This anomaly is very likely to be associated with the frozen core of an adjacent palsa that the ERT profile passes right next to. The second interesting feature is a narrow zone of low resistivity, suggesting an open talik linking the thaw pool between palsa TA-196-2;3, to the groundwater below (Figure 26). The feature is also visible on the 4 m spacing profile over the same palsas.

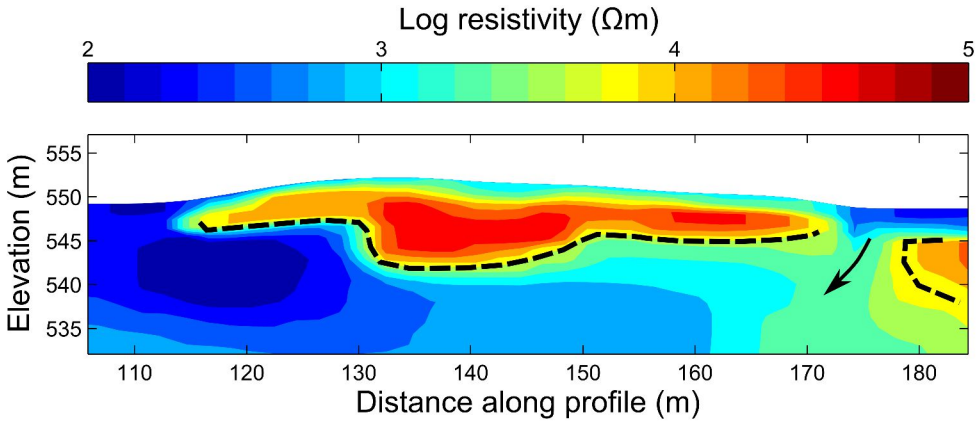

Figure 26: Palsa TA-196-2 interpretation. Dashed line indicating possible extent of permafrost, arrow indicating possible open talik.

The resistivity model of palsa TA-316 shows internal variations of resistivity, from 25000 Ωm in the end of the profile to 45000 Ωm close to the thawing edge (Figure 27). Higher ice content at the edge could be an explanation for these values. Since the edge is closer to the surrounding water body, there is more available water for excess ice formation, which could be one explanation for this difference. The higher resistivity could however also be an effect of less ground contact due to the air-filled crevasses between the eroding blocks of peat at the thawing edge. Since air has an infinite resistivity (Table 1), this can have a large effect on the measured values. The resistivity model also indicates an area of lower resistivity directly below the active layer depth acquired from frost table probings, between x-location 26 – 32 m (Dash-dotted line). This could be due to higher permafrost temperature and thus increased water content directly below the surface. The surface of the palsa was mostly bare over this area, so an increased absorption of incoming solar radiation during the past summer due to the lower albedo of bare peat could be one explanation.

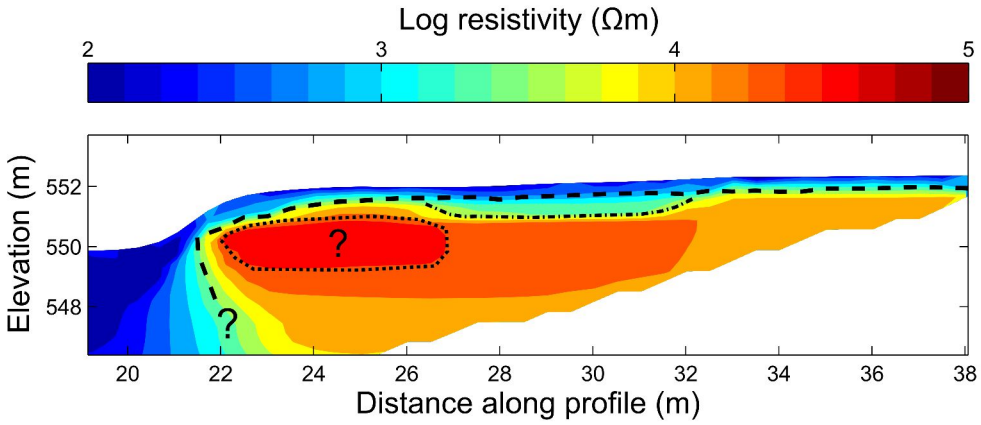

Figure 27: TA-316 Interpretation. Dashed line indicating possible extent of permafrost (from probings and extrapolated), dotted line indicating high resistivity area close to edge, dash-dotted line indicating low resistivity area of shallow permafrost.

A feature suggesting an open talik underneath one of the thaw depression seen on the surface of TA-221 is also visible in the resistivity model between palsa TA-221-1;2 (Figure 28), similar to the observation in TA-196. The model also suggests variations in resistivity close to the surface of the thaw depression at x-location 45 m (Dotted line), similar to the thawed edge at TA-316. This might be due to the presence of thick ice lenses. Low permafrost temperatures which potentially could explain the values are unlikely below the thaw depression where snow accumulates and insulate the ground during winter. This type of sharp resistivity contrast feature could however also be due to the inversion process.

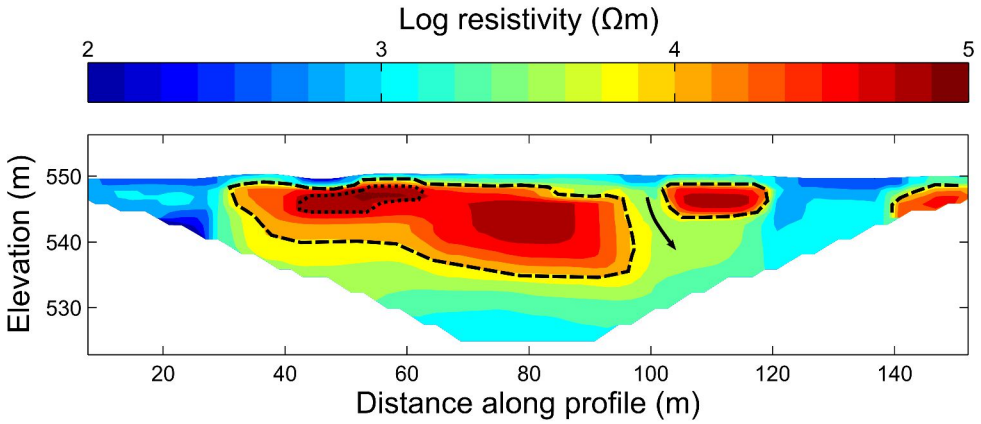

Figure 28: TA-221 Interpretation. Dashed line indicating possible extent of permafrost, dotted line indicating area of high resistivity, arrow indicating possible open talik.

4.4 Distribution and characteristics of permafrost

From the ERT results it seems likely that permafrost is not exclusively confined to only below palsas. Some fens show resistive anomalies underneath that could be interpreted as permafrost as well. These could possibly be the frozen remnants of earlier palsas that have survived due to reasons which are beyond the scope of this study to investigate.

Profile TA-196EX shows a resistive anomaly (visible on TA-196 also) below the fen between x-location 240 – 250 m (Figure 29), suggesting that permafrost is present under the fen. There is also a small space between the resistive blocks possibly constituting the palsa core and the deeper anomaly. This might indicate that the deep ice is decoupled from the palsa core, or it might just be that the inversion routine incorrectly generated this feature. The inversion model of profile TA-196 did not capture the same feature. Speaking in favor of an accurate interpretation of the decoupled block is the EIF value of 0,33, which fits very well according to previously suggested relationships (Allard et al., 1986) of mound height to thickness of permafrost.

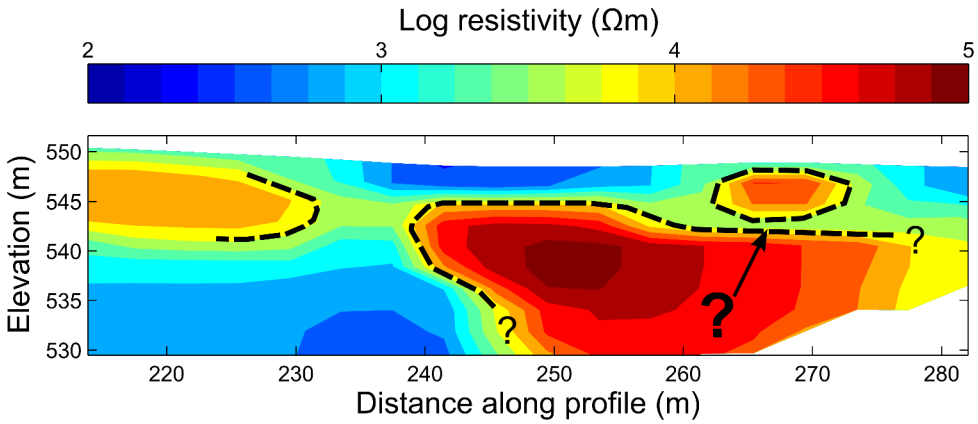

Figure 29: TA-196EX interpretation. Dashed line indicating possible extent of permafrost.

The previously discussed deep resistive anomalies under profile TA-204, especially underneath mounds TA-204-8;11, can probably not fully be explained by the presence of dry and unfrozen resistive sediments. The ground-water level in sediments is likely to be connected to the lake close to the transect (Ylva Sjöberg, personal communication), the deposits should consequently experience saturated conditions to a maximum of a few meters below the surface, and thus be electrically conductive. In the figure below (Figure 30) it is evident that the resistive anomaly below palsas TA-204;8-11 is much deeper than a few meters. The probability that the underlying sediments are unsaturated down to 18

meters is very unlikely, and no other (geo-)logic explanation of the high resistivities other than permafrost can be found. This is assuming that the model fit is reliable. Without ground-truthing here, this remains uncertain.

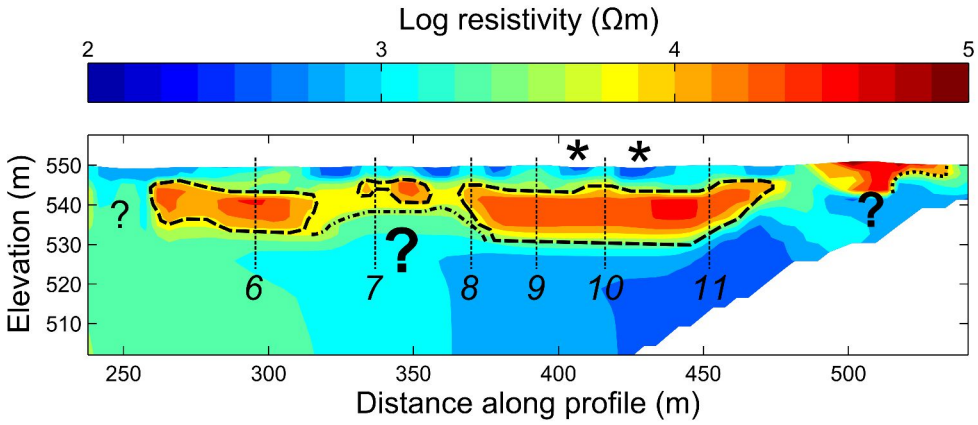

Figure 30: TA-204 Interpretation. Dashed line indicating possible extent of permafrost, dash-dotted line indicating boundary discussed in text, dotted line indicating possible extent of glaciofluvial sediments, stars indicating fens with visible ground-water level at surface.

The same anomaly in the end of the profile underneath mounds TA-204-8;11 is laterally connected joining the frozen cores of all these mounds. Also between TA-204-5;6 a resistive anomaly is underlying the fen. This suggests permafrost underneath four of the fens/thermokarst lakes over the profile, where block erosion is visible on one of them. The ERT profile only passes on the side of the wettest areas however, which could mean that the ERT doesn't capture the possibly thawed bottom of the wet areas. Field observations of visible ground-water surface are made in two of the fens above the resistive block (Figure 30: Indicated by star), but in other depressions along this profile there are no ground-water surfaces observed, and peat seems relatively dry in these depressions, possibly at or below field capacity. There are however no data on peat depth to suggest the entire peat could be below field capacity. Figure 31a shows the ground-water surface of fen between TA-204-9;10, and figure 31b shows the depression between TA-204-6;7. This suggests the possibility of a saturated area confined by the underlying ice between palsas 8-11.

a)

b)

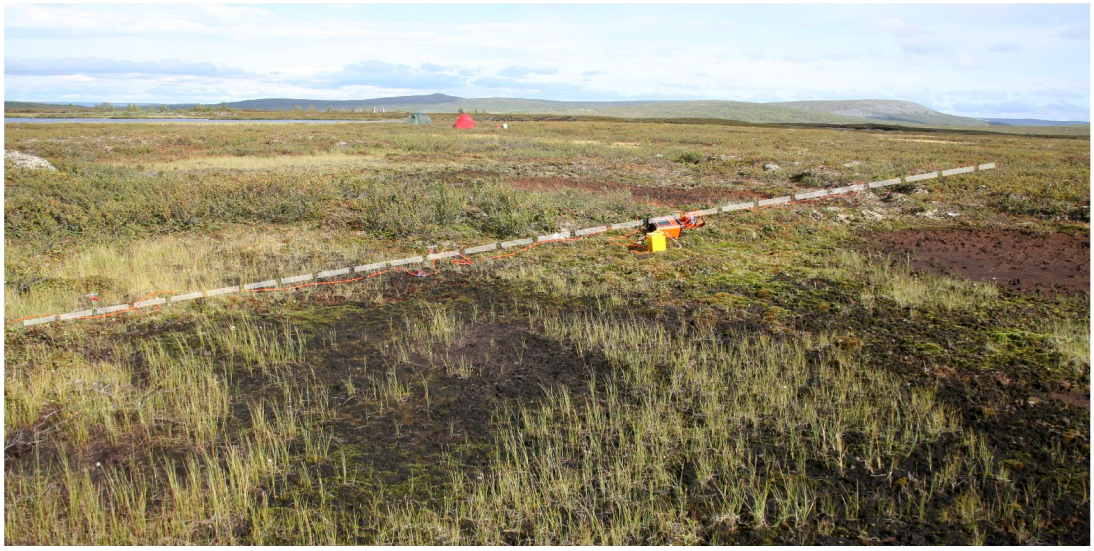

Figure 31: Profile TA-204. a) Fen with visible ground-water surface between TA-204-9;10 b) Low resistivity depression between TA-204-6;7 with no ground-water surface observed.

The shallowing and weakening of lower resistivity interface at approximately x-location 350 m (Figure 30: Indicated by dash-dotted line) could possibly indicate saturated non-frozen sediments below with unfrozen moist sediments above, possibly glaciofluvials, but this is only speculative. The interface is however likely to be too deep to be a ground-water level, but this could be due to the inversion process. The hypothesized section of drier sediments above this line (but likely a lot shallower than the model suggests) is supported by the observation of relatively dry overlying peat where soil water might not percolate downwards to fill pore-spaces of the underlying sediments, thus by

Archie´s law (E.g. Reynolds, 2011) this target should be more resistive. The suggestion is illustrated by a simple model below (Figure 32). An unknown component of this interpretation, in addition to unknown actual ground-water levels, is if the shallow permafrost within the peat found by physical probings actually is connected to the deeper permafrost found in the resistivity model. Another explanation to this medium resistive area could be the influence of a frozen core of an adjacent peat plateau.

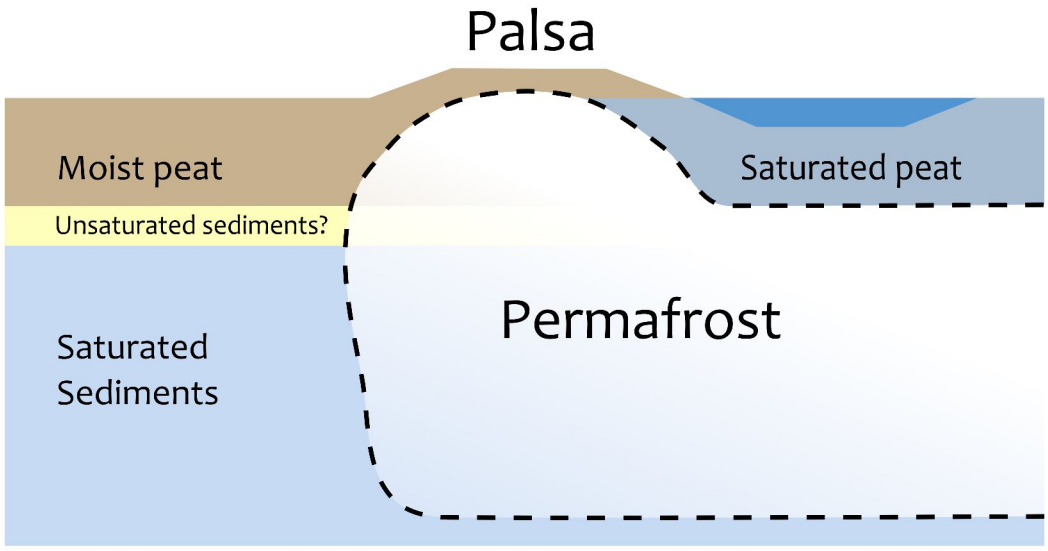

Figure 32: Conceptual model of interpretation discussed in text.

The interpretation of deep frozen sediments of TA-204 is complicated by the previously discussed relationship of increasing resistivity closer to the glaciofluvial ridge (See figure 24). Since sediments are thought to be frozen, low amounts of segregated ice should yield a lower resistivity for the non-frost-susceptible glaciofluvial sediments. Maybe the presence of gas filled pore spaces in the frozen sediments could explain the increasing resisitivities. The 8 m deep resistive anomaly under the glaciofluvial ridge is also hard to explain since water from the adjacent lake easily should infiltrate the deposit and make it conductive well above this limit.

Permafrost thickness ranges from 5 to 17 m, with the thickest permafrost on the western end on profile TA-204, while the highest mounds are found on the eastern end of the study area where permafrost is less deep. A power regression was fitted to the data to explain the relationship (Figure 33), expressed by the following equation

$$t = -22 + 35 \cdot h^{-0,15} \quad (17)$$

where t is permafrost thickness and h is mound height, with an r^2 of 0,39. This result is in major contrast to previous findings of Allard et al. (1986), who found mound height increasing with permafrost thickness by a factor of approximately 1/3, in Québec, Canada.

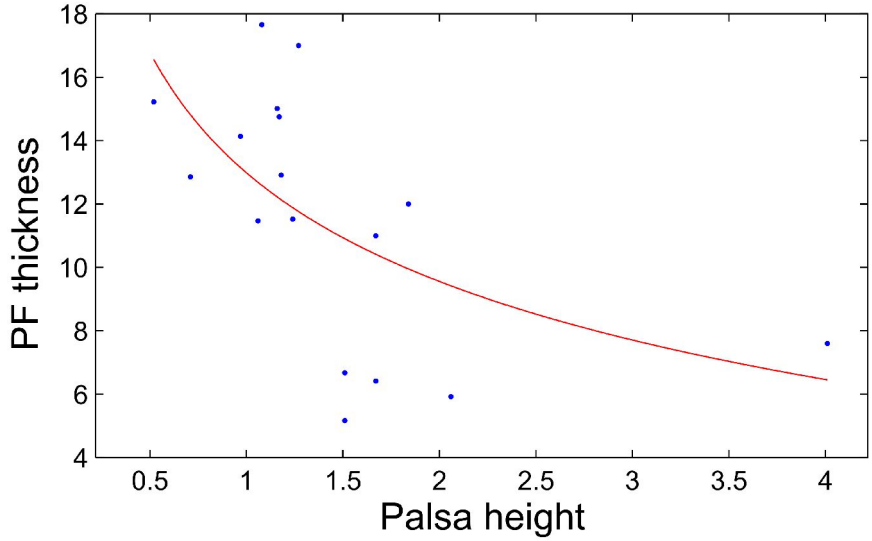

Figure 33: Permafrost thickness vs. Mound height. Red line shows permafrost thickness as a function of mound height.

The explanation for this difference in results might be the presence of less frost susceptible sediments in the west end of the study area, which allowed for deep frost penetration without excessive ice segregation formation. This could produce smaller mounds with deep permafrost underneath. The results from this study thus suggests that the relationship between palsa size and permafrost thickness is complex under heterogenic ground conditions, but further studies needs to be carried to explain the relationships.

4.5 Some notes on ERT uncertainty

The ambiguity of geophysical data always has to be considered when interpreting the results of any geophysical survey (E.g. Roy, 1962). The geological model derived after inversion modeling is not unique, small or large deviations from reality will always occur in the model using the techniques existing today. This means that one of several different sets of inverted models from a 2-dimensional electrical resistivity survey can fit the observations in apparent resistivity measured at the surface just as well as any of the other

models. Picking the right model is not easy, particularly when the sub-surface is hard to predict, as in the case of a palsa bog, and where few physical observations are available this is even more difficult.

The high resistivity contrasts in the palsa bog pose a special challenge for inversion modeling, as the probability for errors in the model increase with increased resistivity contrast (Dahlin and Loke, 1998). This has been shown in a permafrost environment by Hilbich et al. (2009) using the DOI method (Oldenburg and Li, 1999), where high resistivity contrasts made interpretations of the depth to base of permafrost in ice-rich rock glaciers uncertain. This problem was mitigated during this master thesis by using the Gauss-Newton method for inversion which produces better results when the sub-surface shows large contrasts in resistivity (Loke and Dahlin, 2002). The spatial model uncertainties were also qualitatively assessed before interpretation. Most profiles were also measured with the survey line extending as far as possible away from the surveyed mounds to increase the resolution at depth below palsas.

The sensitivity of inversion resistivity modeling in the palsa bog environment have yet been assessed however, thus research is needed here. Since the conditions and ground composition are much different in the palsa bog compared to the mountain permafrost environment where most studies considering the ERT reliability have been conducted (E.g. Hilbich et al., 2009), it is not possible to say if the reliability ranges are in the same range in the palsa bog without research on this topic.

5 CONCLUSIONS

The main conclusion of this study is that ERT can be used to investigate permafrost thickness, possibly the variations in ice content, and also the details of palsa internal structure, in the palsa bog environment. The values of these acquired parameters are similar to those found by Lewkowicz et al. (2011) using the same geophysical method in Yukon, Canada.

Other important observations are also that permafrost might not be confined exclusively to palsas and peat plateaus, but could likely also occur at depth underneath some of the fens. Low (< 1,5 m) peat-plateaus with thermokarst lakes were found be to underlain by deep (> 15 m) resistive anomalies, likely to be permafrost. Thawing of palsas could not be confirmed during the scope of this study by the relatively limited ERT data, but possible signs of thawing from the side and from below are found under one palsa (TA-196-2).

Variations in shallow permafrost resistivity could be detected on the top of palsas using a shorter 0,5 m spacing, likely indicating varying ice-water content attributed to differential warming of permafrost. This demonstrates that ERT is an excellent tool to investigate near-surface processes on palsas, where the sensitivity of the method is high. Significant variation in calculated excess ice content were also found amongst the palsas and peat plateaus, and this is possibly due to heterogenic ground underlying the mounds of the area.

Permafrost depths determined by ERT measurements are always uncertain and ambiguous, especially in areas with high resistivity contrasts (Dahlin and Loke, 1998). The ERT depth to permafrost base under one palsa (TA-196-2) acquired from two ERT profiles compared to temperature data from one borehole suggests that permafrost thicknesses in the palsa bog might be underestimated by the inversion process.

Mound height was found to decrease with the thickness of permafrost acquired by ERT. This is a result that was not expected before hand, due to the processes described in the literature regarding palsa development (E.g. Seppälä, 1986) and previously described relationships (Allard et al., 1986). This relationship is possibly due to large variations in the contents of excess ice under the mounds. Especially low values, thus small amounts of frost heave (French, 2007), are suggested to be attributed to (frozen) glaciofluvial sediments under low peat plateaus. This study consequently suggests that the relationship between palsa size and permafrost thickness is complex under heterogenic ground conditions, where excess ice formation capacities of the underlying material is not uniform. These findings cannot be verified without further studies however, and the

author stands careful in drawing conclusions only upon the basis of the single ERT depth measurements. The possibility of the frozen cores of the peat plateaus being connected to the deeper permafrost under profile TA-204 also remains to be answered.

6 Acknowledgements

I am very thankful for all the support my supervisors Ylva Sjöberg (Stockholm University) and Rickard Pettersson (Uppsala University) have given me during this work. A special thanks also goes to Matthias Siewert (Stockholm University), who not only assisted me in the field, but also tutored me on using the ABEM Lund system, and later gave valuable tips and ideas on how to address the data processing and inversion. I also thank Britta Sannel at SU for help with questions regarding the boreholes in Tavvavuoma.

Next thanks goes to Maria García Juanatey at the department of geophysics (Uppsala University) for some help getting started with the interpretation methodology while Rickard was away on field work. I also send a thanks to Chunling Chan at the same department for help with some of the first rows of scripting in Matlab.

I thank Bernd Etzelmüller at the University of Oslo for giving me the opportunity to join the excursion to Raubergstulen in June 2012 where I first got in contact with my supervisor Ylva to make this project.

The equipment used for the ERT survey, as well as the inversion software, was kindly lent out by the department of geophysics at Uppsala University.

7 References

ABEM Instrument AB. (2012). *ABEM Terrameter LS, Instruction manual*. ABEM Instrument AB, Sweden.

Allard, M., Seguin, M.K., Levesque, R. (1986). Palsas and mineral permafrost mounds in northern Quebec. - In: I*nternational Geomorphology, Proceedings of the first international conference on Geomorphology, Part II,* Gardiner V (ed). John Wiley and Sons Ltd, Chichester, 285–309.

Brown, J., Ferrians, O.J.J., Heginbottom, J.A. and Melnikov, E.S. (1997). *International Permafrost Association Circum-Arctic Map of Permafrost and Ground Ice Conditions, Scale 1:10,000,000*. U.S. Geological Survey.

Christiansen, H.H., et al. (2010). The Thermal State of Permafrost in the Nordic Area during the International Polar Year 2007–2009. *Permafrost and Periglacial Processes* 21, 156-181.

Dahlin, T., and Loke, M.H. (1998). Resolution of 2D Wenner resistivity imaging as assessed by numerical modelling. *Journal of Applied Geophysics* 38, 237-249.

Dey, A., and Morrison, H.F. (1979). Resistivity modelling for arbitrary shaped two-dimensional structures. *Geophysical Prospecting* 27, 106-136.

Etzelmüller, B., Heggem, E.S.F., Sharkhuu, N., Frauenfelder, R., Kääb, A., Goulden, C. (2006). Mountain permafrost distribution modelling using a multi-criteria approach in the Hövsgöl area, northern Mongolia. *Permafrost and Periglacial Processes* 17, 91-104.

Hauck, C., Isaksen, K., Vonder Mühll, D., Sollid, JL. (2004). Geophysical surveys designed to delineate the altitudinal limit of mountain permafrost: an example from Jotunheimen, Norway. *Permafrost and Periglacial Processes* 15, 191-205.

Hauck, C. and Kneisel, C. (2008). *Applied Geophysics In Periglacial Environments*. Cambridge University Press, Cambridge, UK.

Hempel, L. (2009). *The Holocene development of the Tavvavuoma peat plateau based on plant macrofossil analysis.* B.Sc. Thesis, 18 pp., Department of Physical Geography and Quarternary Geology, Stockholm Univiversity, Stockholm.

Hendriks, M.R. (2010). *Introduction to physical hydrology*. Oxford University Press, New York.

Hilbich, C., Marescot, L., Hauck, C., Loke, M.H., Mausbacher, R. (2009).

Applicability of electrical resistivity tomography monitoring to coarse blocky and ice-rich permafrost landforms. *Permafrost and Periglacial Processes* 20(3), 269–284.

Hohmann, M. (1997). Soil freezing — the concept of soil water potential. State of the art. *Cold Regions Science and Technology* 25, 101–110.

Isaksen, K., Hauck, C., Gudevang, E., Ødegård, R.S., Sollid, J.L. (2002). Mountain permafrost distribution on Dovrefjell and Jotunheimen, southern Norway, based on BTS and DC resistivity tomography data. *Norsk Geografisk Tidsskrift* 56, 122-136.

Ivanova, N.V., Kuznetsova, I.L., Parmuzin I.S., Rivkin F.M., Sorokovikov V.A. (2011). Geocryological Conditions Swedish Lapland. Fundamentproect OJSC, Moscow, Russia. - In: *Proceeding of the Fourth Russian Geocryology Conference,* Volume 2, Part 5, 77-82. University press, Moscow.

Kneisel, C., Hauck, C., Vonder Mühll, D. (2000). Permafrost below the timberline confirmed and characterized by geoelectrical resistivity measurements, Bever Valley, eastern Swiss Alps. *Permafrost and Periglacial Processes* 11, 295-304.

Kneisel, C., Hauck, C., Fortier, R., and Moorman, B. (2008). Advances in Geophysical Methods for Permafrost Investigations. *Permafrost and Periglacial Processes* 19, 157-178.

Kneisel, C., Sæmundsson, Þ., and Beylich, A.A. (2007). Reconnaissance surveys of contemporary permafrost environments in central Iceland using geoelectrical methods: implications for permafrost degradation and sediment fluxes. *Geografiska Annaler* 89A, 41-50.

Kristensen, L., Juliussen, H., Christiansen, H. H. and Humlum, O. (2009). Structure and composition of a tidewater glacier push moraine, Svalbard, revealed by DC resistivity profiling. *Boreas* 38, 176-186.

Lagerbäck, R. (2012). *Map of the Quarternary deposits of northernmost Sweden, north-eastern part, scale 1:250 000*. Sveriges Geologiska Undersökning, K422:2.

Lewkowicz, A.G., Etzelmüller, B., Smith, S.L. (2011). Characteristics of Discontinuous Permafrost based on Ground Temperature Measurements and Electrical Resistivity Tomography, Southern Yukon, Canada. *Permafrost and Periglacial Processes* 22, 320-342.

Loke, M.H. (2001). *Tutorial: 2-D and 3-D electrical imaging surveys*. (Revised 2012). Geotomo Software, Malaysia.

Loke, M.H. (2010). *RES2DINV ver. 3.59: Rapid 2-D Resistivity & IP inversion using the least-squares method*. Geotomo Software, Malaysia.

Loke, M.H., and Dahlin, T. (2002). A comparison of the Gauss–Newton and quasi-Newton methods in resistivity imaging inversion. *Journal of Applied Geophysics* 49, 149-162.

Lundqvist, J. (1969). Earth and ice mounds: a terminological discussion. – In: Pewe, T.L. (ed.) *The Periglacial Environment. Past and Present*, 203-215. McGill-Queen's University Press, Montreal.

Naturvårdsverket. (2008). *Nationalparksplan för Sverige: Genomförande 2009-2013*. Naturvårdsverket, Rapport 5839, ISBN 978-91-620-5839-5.

Oldenburg, D.W., and Li, Y. (1999). Estimating depth of investigation in DC resistivity and IP surveys. *Geophysics* 64, 403-416.

Pissart, A. and Gangloff, P. (1984). Les palses minérales et organiques de la vallée de l'Aveneau, prés de Kuujjuaq, Québec subarctique. *Géographie Physique et Quaternaire* 38, 217-28.

Pissart, A. (2002). Palsas, lithalsas and remnants of these periglacial mounds: a progress report. *Progress in Physical Geography* 26, 605-621.

Rapp, A., Annersten, L. (1969). Permafrost and tundraplolygons in northern Sweden. – In: Pewe, T.L. (ed.) *The Periglacial Environment. Past and Present*, 65-91. McGill-Queen's University Press, Montreal.

Reynolds, J.M. (2011). *An Introduction to Applied and Environmental Geophysics*. 2nd Ed. John Wiley & Sons, UK.

Rivkin, F.M. (2009). *The Tavvavuoma Area Geocryological Map and Characteristics of Geocryological Conditions. Explanatory Notes to Permafrost Map of Tavvavuoma Region (Sweden).* Science and education program: Field mapping and geophysical research methods in subarctic permafrost regions (GEOPERM). OJSC Fundamentproekt, Moscow.

Ross, N., Brabham, P.J., Harris, C., Christiansen, H.H. (2007). Internal structure of open system pingos, Adventdalen, Svalbard: the use of resistivity tomography to assess ground-ice conditions. *Journal of Environmental and Engineering Geophysics* 12, 113-126.

Roy, A. (1962). Ambiguity in Geophysical Interpretation. *Geophysics* 27, 90-99.

Sannel, A. B. K., and Kuhry, P. (2011). Warming-induced destabilization of peat plateau/thermokarst lake complexes. *Journal of Geophysical Research* 116, G03035.

Seppälä, M. (1972). The term 'palsa'. *Zeitschrift für Geomorphologie* 16, 463.

Seppälä, M. (1986). The origin of Palsas. *Geografiska Annaler* 68 A (3), 141-147.

Seppälä, M. (1988). Palsas and related forms. In: Clark, M.J. (Ed.), *Advances in Periglacial Geomorphology,* 247–278. John Wiley, Chichester.

Seppälä, M. (2011). Synthesis of studies of palsa formation underlining the importance of local environmental and physical characteristics. *Quaternary Research* 75, 2, 366–370.

Silvester, P.P. and Ferrari, R.L. (1990). *Finite elements for electrical engineers* (2nd. ed.). Cambridge University Press.

Sollid J.L., and Sørbel, L. (1998). Palsa Bogs as a Climate Indicator: Examples from Dovrefjell, Southern Norway. *Ambio* 27, No. 4, 287-291.

Stummer, P. (2003). *New Developments in Electrical Resistivity Imaging*. Ph.d. Thesis. Swiss Federal Institute of Technology Zurich. Diss. ETH no. 15034.

Ulfstedt, A.C. (1982). *Geomorfologiska kartbladet 32 J Treriksröset 32 K Kummavuopio 31 J Råstojaure 31 K Naimakka – Beskrivning och naturvärdesbedömning*. Naturvårdsverket, SNV PM 1555.

Van Everdingen, R. (ed.) (1998). *Multi-language glossary of permafrost and related ground-ice terms*. (Revised May 2005). National Snow and Ice Data Center/World Data Center for Glaciology, Boulder, CO, USA.

Wramner, P. (1965). Fynd av palsar med mineraljordskärna i Sverige. *Geologiska Föreningens Förhandlingar* 86, 498-499.

Wramner, P. (1968). *Studier av palsmyrar i Taavavuoma och Laivadalen, Lappland*. Lic. Thesis. Göteborgs University.

Wramner, P. (1972). *Palslika bildningar i mineraljord. Några iakttagelser från Taavavuoma, Lappland*. Göteborgs University, GUNI Rapport 1.

Wramner, P. (1973). *Palsmyrar i Taavavuoma, Lappland*. Göteborgs University, GUNI Rapport 3.

Yoshikawa, K., Leuschen, C., Ikeda, A., Harada, K., Gogineni, P., Hoekstra, P., Hinzman, L., Sawada, Y., and Matsuoka, N. (2006). Comparison of geophysical investigations for detection of massive ground ice (pingo ice). *Journal of Geophysical Research* 111, E06S19.

Zuidhoff, F.S. (2003). *Palsa growth and decay in Northern Sweden: Climatic and Environmental Controls*. Acta Universitatis Upsalensis. Comprehensive Summaries of Uppsala Dissertations from the Faculty of Science and

Technology, 813, 30 pp. Uppsala.

Zuidhoff, F.S, and Kolstrup, E. (2000). Changes in Palsa Distribution in Relation to Climate Change in Laivadalen, Northern Sweden, Especially 1960-1997. *Permafrost and Periglacial Processes* 11, 55-69.

Åhman, R. (1977). *Palsar i Nordnorge: En studie av palsars morfologi, utbredning och klimatiska förutsättningar i Finnmarks och Troms fylke*. Ph.D Thesis, Lund.

7.1 Internet sources

Swedish Meteorological and Hydrological Institute (SMHI). http://www.smhi.se/klimatdata. (Accessed 2013-01-29, and 2013-05-14)

The Geological Survey of Sweden (SGU). http://maps2.sgu.se/kartgenerator/maporder_sv.html. (Accessed 2013-02-01)

Appendix I: Model uncertainty plots

TA-196EX inversion model (above) and model uncertainty (below).

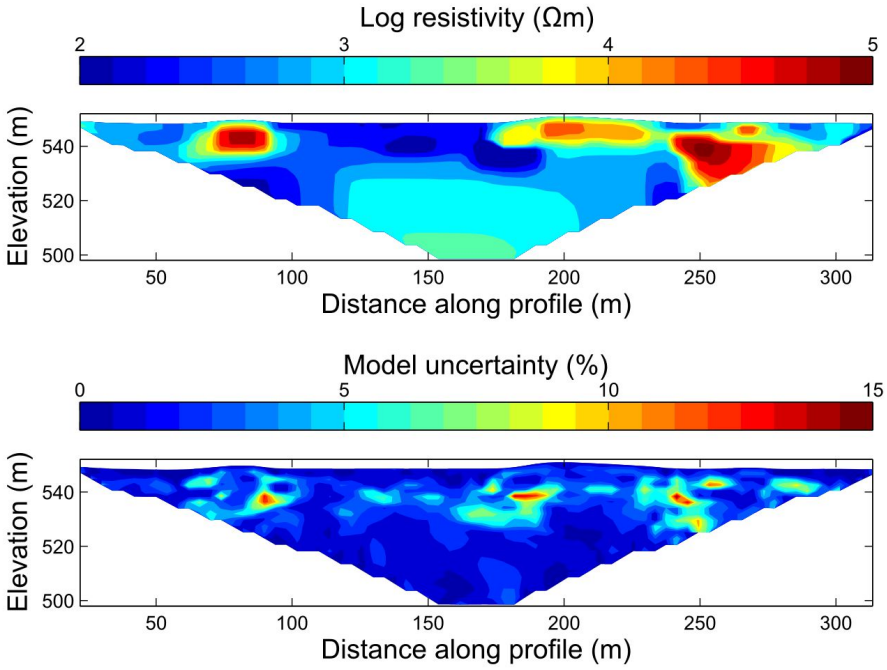

TA-204 inversion model (above) and model uncertainty (below).

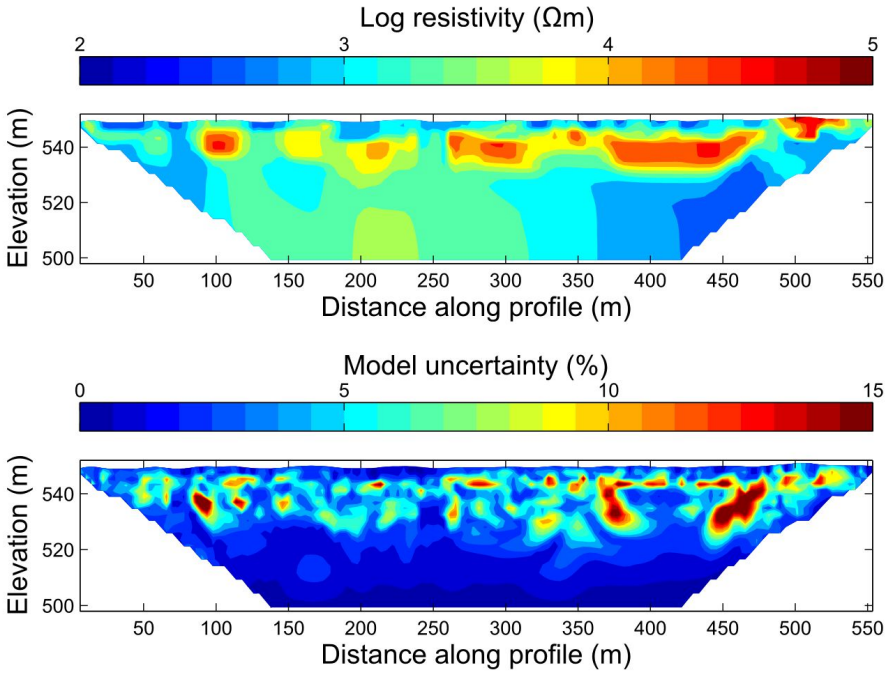

TA-221 inversion model (above) and model uncertainty (below).

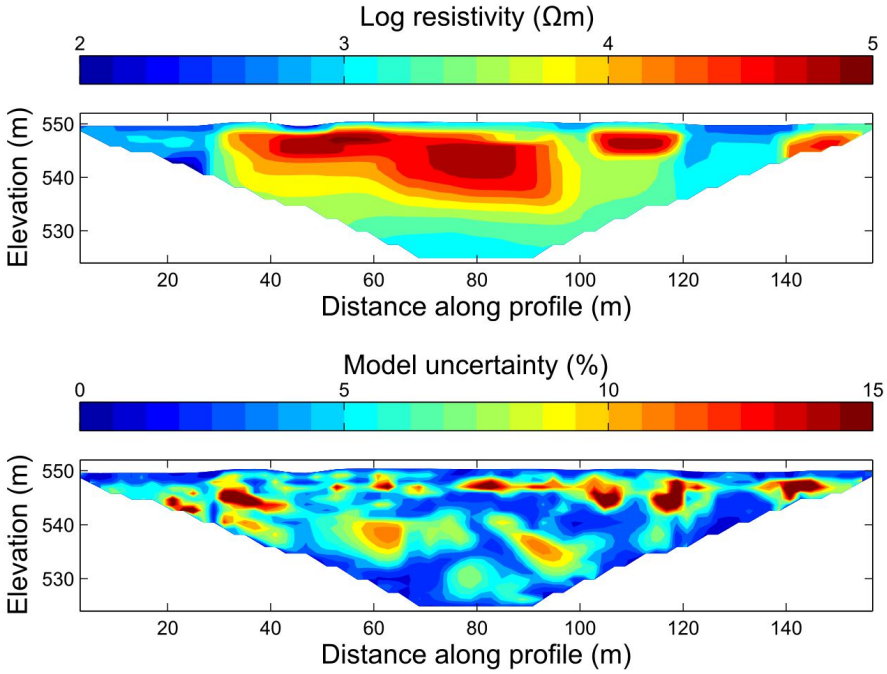

TA-316 inversion model (above) and model uncertainty (below).

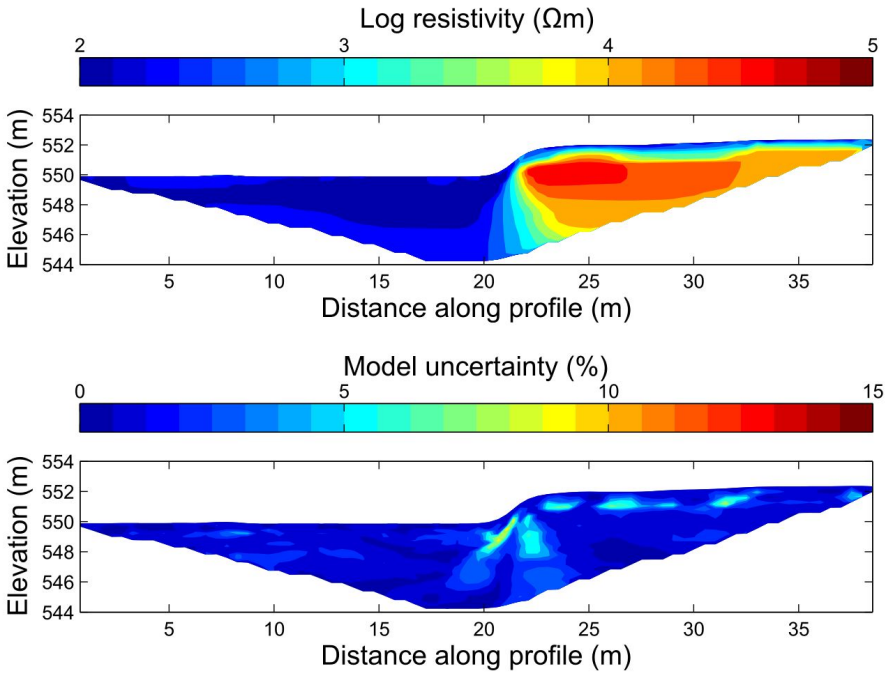

Appendix II: Inverse model, synthetic- and measured apparent resistivity plots

TA-196

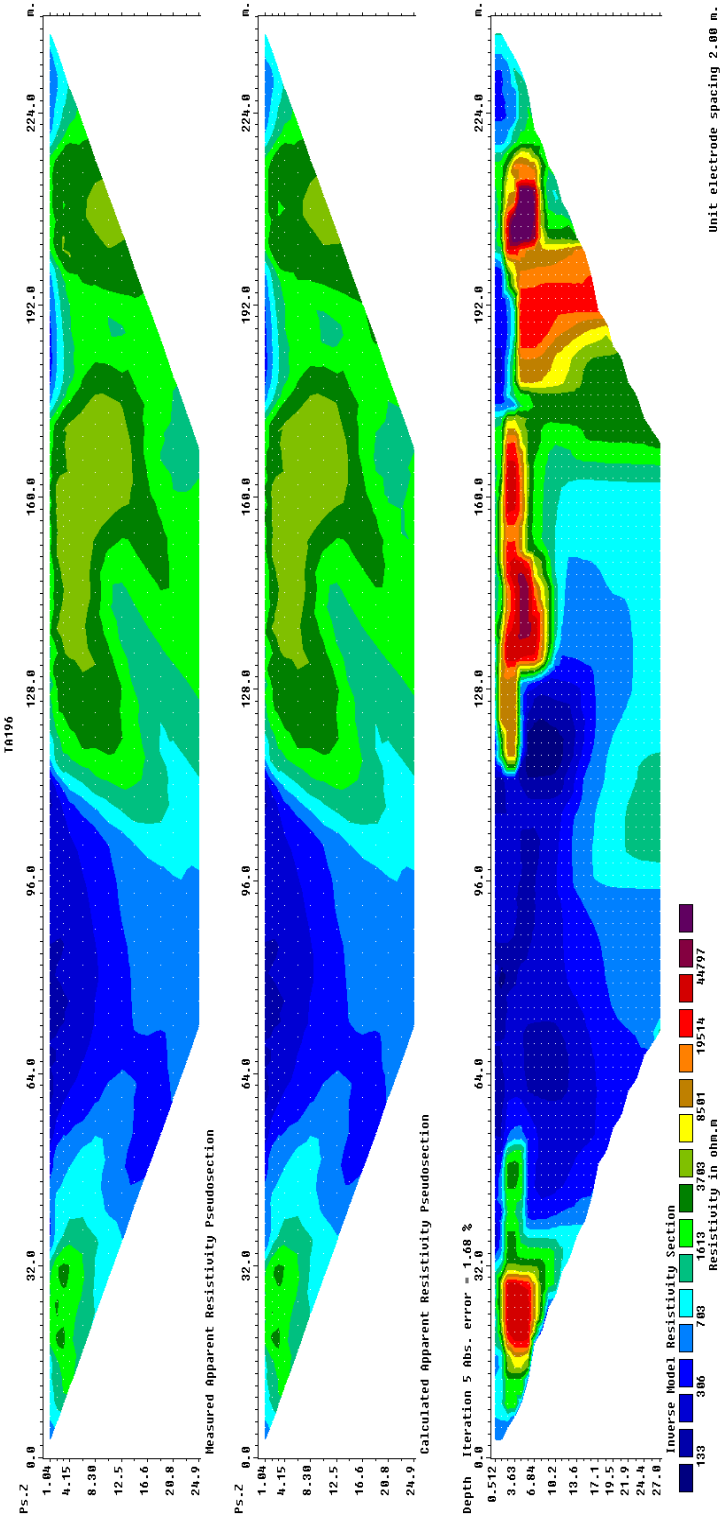

TA-196EX

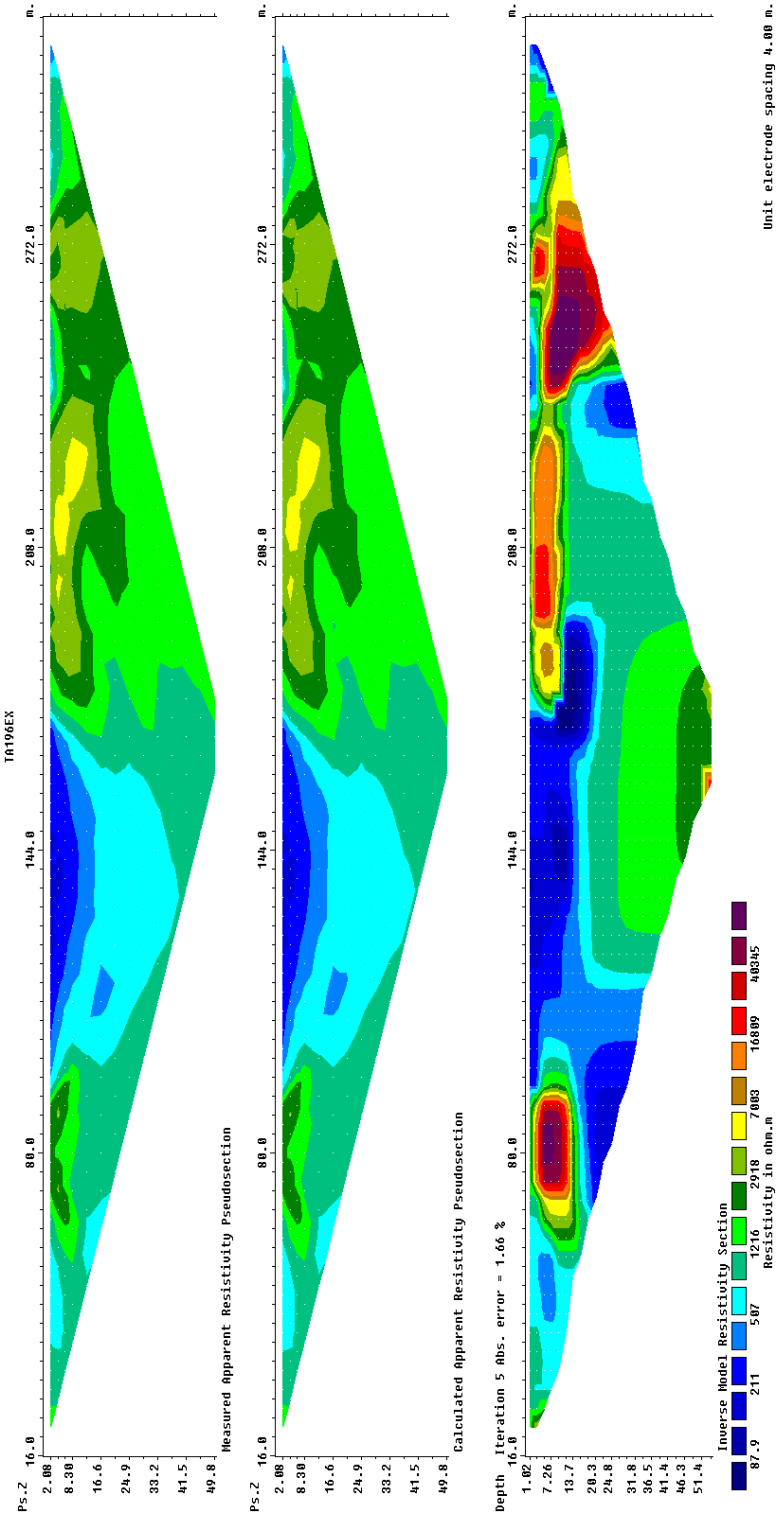
TA196EX
Measured Apparent Resistivity Pseudosection
Calculated Apparent Resistivity Pseudosection
Inverse Model Resistivity Section
Resistivity in ohm.m
Unit electrode spacing 4.00 m.
Iteration 5 Abs. error = 1.66 %

TA-204

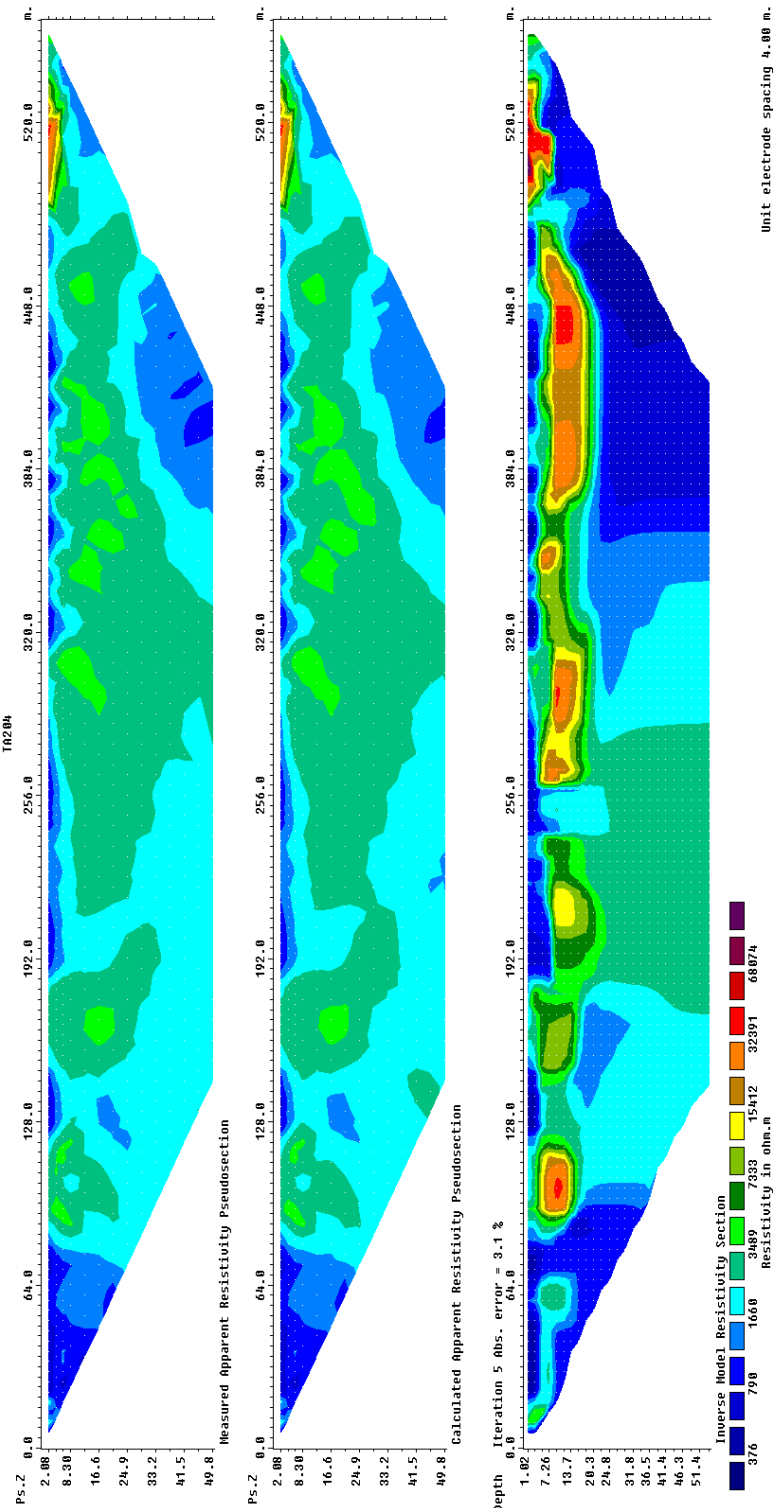
TA204
Ps.z
0.0
2.08
8.30
16.6
24.9
33.2
41.5
49.8
m.
0.0
64.0
128.0
192.0
256.0
320.0
384.0
448.0
520.0
Measured Apparent Resistivity Pseudosection
Calculated Apparent Resistivity Pseudosection
Depth
Iteration 5 Abs. error = 3.1 %
0.0
1.82
7.26
13.7
20.3
24.8
31.8
36.5
41.4
46.3
51.4
Inverse Model Resistivity Section
376
798
1660
3489
7333
15412
32391
68074
Resistivity in ohm.m
Unit electrode spacing 4.00 m.

TA-221

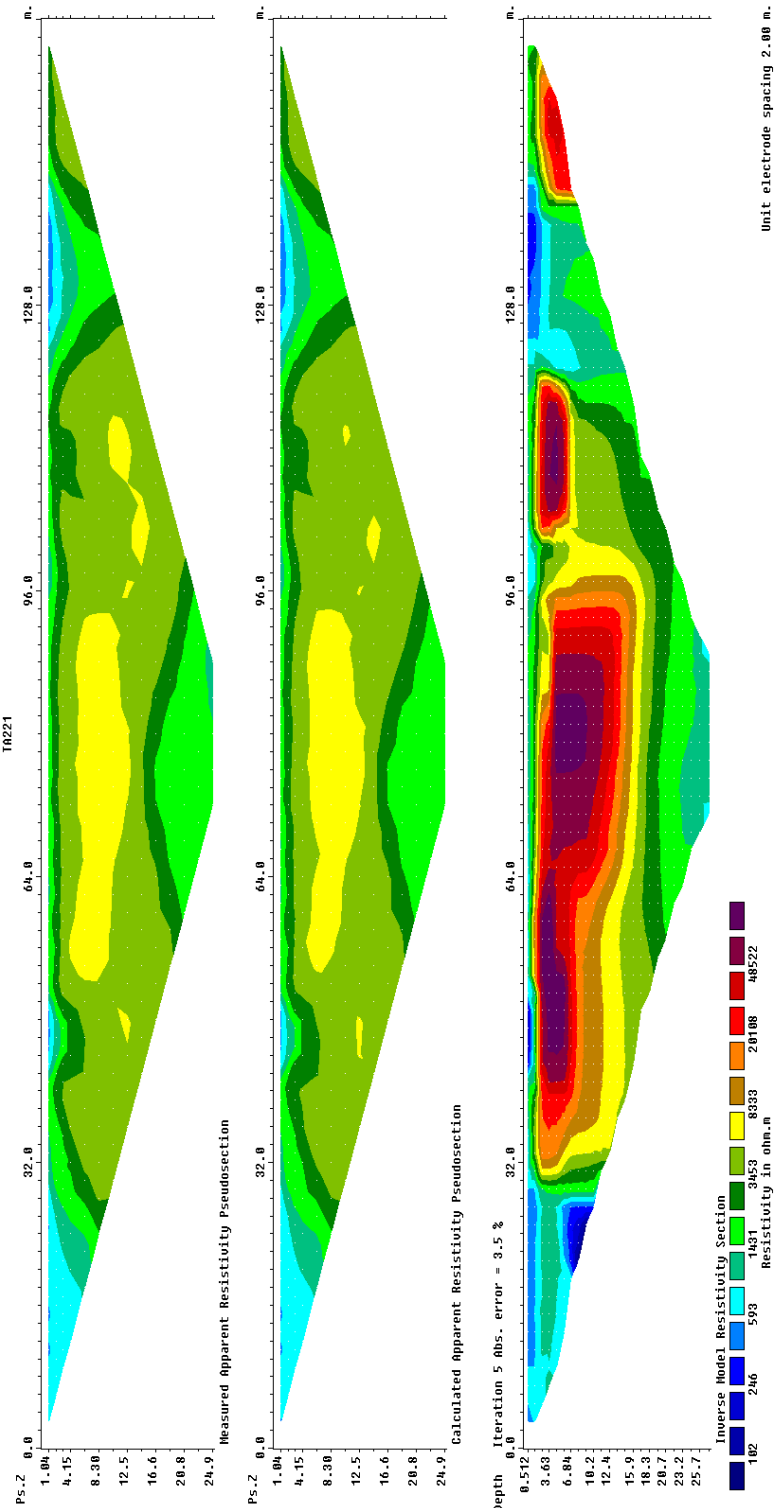
TA221
Measured Apparent Resistivity Pseudosection
Calculated Apparent Resistivity Pseudosection
Inverse Model Resistivity Section
Iteration 5 Abs. error = 3.5 %
Resistivity in ohm.m
Unit electrode spacing 2.00 m.

TA-316

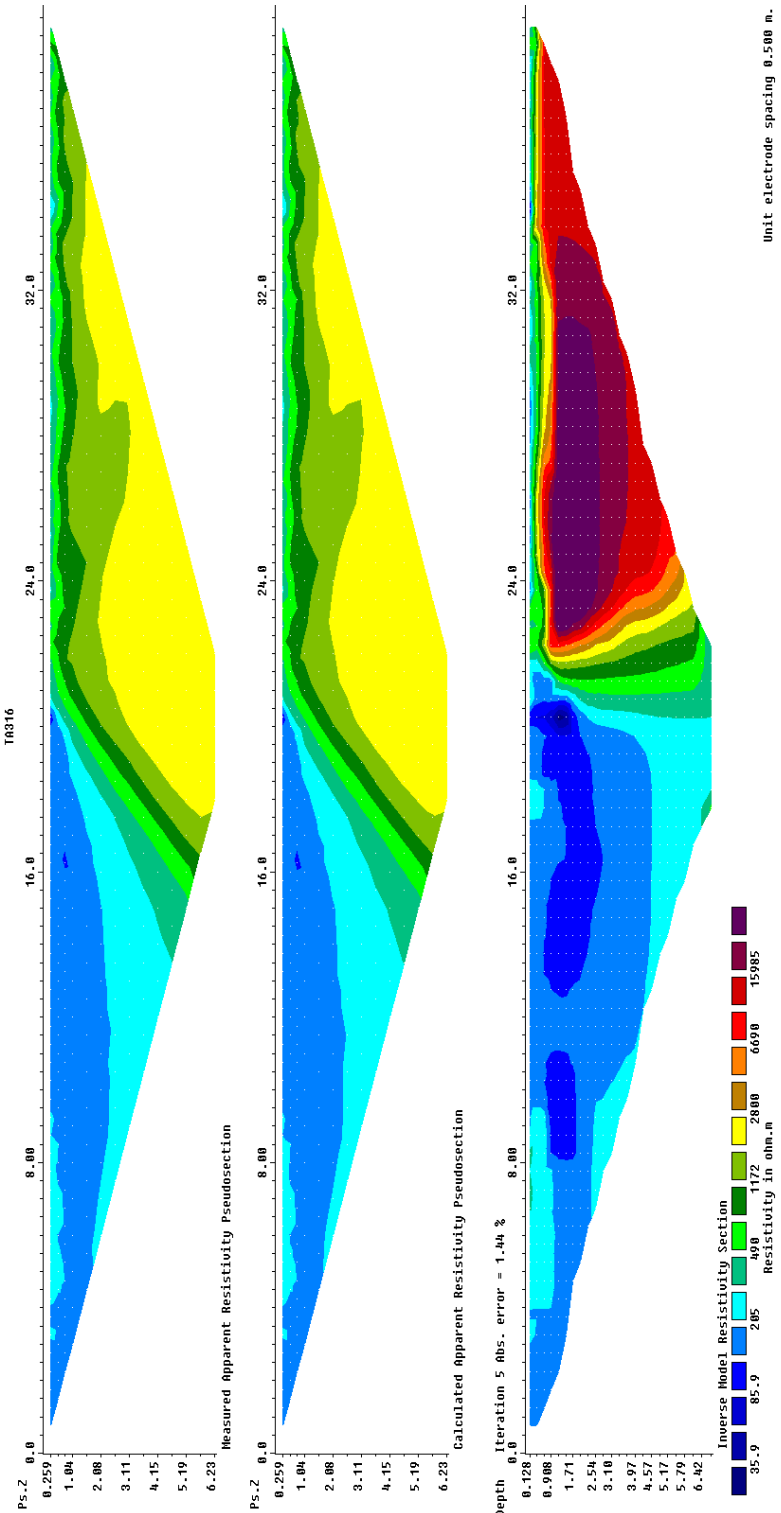
TA0316
Ps.z
0.0
0.259
1.04
2.08
3.11
4.15
5.19
6.23
8.00
16.0
24.0
32.0
Measured Apparent Resistivity Pseudosection
Calculated Apparent Resistivity Pseudosection
Depth
Iteration 5 Abs. error = 1.44 %
0.128
0.908
1.71
2.54
3.10
3.97
4.57
5.17
5.79
6.42
Inverse Model Resistivity Section
35.9
85.9
205
490
1172
2800
6690
15985
Resistivity in ohm.m
Unit electrode spacing 0.500 m.

Appendix III: Field conditions

Weather observations from notebook.

2012-08-21
Sunny / partly cloudy, 15 – 10°C. Last days seems to have been dry, with relatively dry ground conditions as result.

2012-08-22
Overcast, rain during night. Clearing skies on the afternoon. ≈ 10°C.

2012-08-23
Overcast, light drizzle rain. Rain during night. ≈ 8°C

2012-08-24
Fine weather, 70% cloudcover. Enough wind to keep mosquitos away.

2012-08-25
Fine weather, sunny. ≈ 10°C. Weak aurora borealis activity during the previous night.